MULLET

AIAA Design, Build, Fly
Design Report
2021-2022

Table of Contents

Nomenclature

Units

A	Amps
deg	Degrees
fpm	Feet per Minute
ft	Feet
ft/s	Feet per Second
g	Acceleration Under Gravity
h	Hours
in	Inches
lb	Pounds
mAh	Milliamp-hours
min	Minutes
mm	Millimeters
psi	Pounds per Square Inch
rpm	Rotations per Minute
s	Seconds
V	Volts
W	Watts
Wh	Watt-hours

Symbols

b	Span
c	Chord
C_D	Drag Coefficient
C_L	Lift Coefficient
C_M	Pitching Moment Coefficient
L	Lift
L/D	Lift to Drag
n	Load Factor
Q	Dynamic Pressure
Re	Reynolds Number
S	Surface Area
t/c	Thickness to Chord
v	Airspeed
W	Weight
α	Angle of Attack
δ	Control Deflection
ρ	Air Density

Subscripts

e	Elevator
OGE	Out of Ground Effect
W	Wing
wf	With Flaps
wp	With Power

Abbreviations

AC	Aerodynamic Center
AGL	Above Ground Level
AIAA	American Institute of Aeronautics and Astronautics
AOC	Angle of Climb
BHP	Brake Horsepower
BL	Buck Line
CAD	Computer Aided Design
CG	Center of Gravity
COTS	Commercial Off-the-Shelf
DBF	Design, Build, Fly
ERAU DB	Embry-Riddle Aeronautical University Daytona Beach
ESC	Electronic Speed Control
FEA	Finite Element Analysis
FS	Fuselage Station
GM	Ground Mission
HT	Horizontal Tail
M#	Mission #
MAC	Mean Aerodynamic Chord
MLG	Main Landing Gear
MSL	Mean Sea Level
MULLET	Medical Unmanned Low-Level Electric Transport
NLG	Nose Landing Gear
ROC	Rate of Climb
UAV	Unmanned Aerial Vehicle
VSSM	Vaccine Syringe Storage Mechanism
VT	Vertical Tail
VVPDM	Vaccine Vial Package Deployment Mechanism
WL	Water Line

1 Executive Summary

MULLET, the Medical Unmanned Low-Level Electric Transport, is Embry-Riddle Aeronautical University Daytona Beach's aircraft for the 2021–2022 AIAA Design, Build, Fly competition. This UAV was designed to perform four missions, including a ground mission and three flight missions. Mission 1 is a deployment flight that demonstrates the aircraft's flight capability; Mission 2 is a staging flight for the transportation of vaccine syringes; Mission 3 is a delivery flight for the transportation and deployment of vaccine vial packages; and the Ground Mission is a demonstration of the ability to rapidly prepare the aircraft for flight.

The aircraft was designed, manufactured, and flown by a team of 40 undergraduate aerospace engineering students. The design process comprised three phases: conceptual, preliminary, and detail design. Initially, the conceptual design focused on analyzing the requirements with a scoring analysis to select the optimal payload that maximized the mission scores. After the aircraft and subsystem configurations were selected, the weight, wing, tail, and propulsion system were sized during the preliminary design. Sizing trade studies were followed by a detailed analyses of takeoff performance, drag, and stability and control. A detail design then focused on the aircraft's structural characteristics and systems integration. The manufacturing process followed with the goal of fabricating the aircraft to the designed specifications and weight. A detailed schedule was developed and was continuously refined to manufacture each aircraft iteration in a timely manner, enabling rapid prototyping throughout the design, build, and fly process. Finally, a testing plan was established to evaluate a series of test objectives essential to the aircraft's mission performance.

MULLET's design, shown in Figure 1-1, features a conventional, low-wing, single-engine tractor configuration that optimizes the mission scores under the primary limits imposed by the 25-ft takeoff distance and stored propulsion energy of 100 Wh. The wing provides ample lift capability and the motor produces sufficient thrust for takeoff at maximum gross weight. The internal fuselage volume allows adequate room to store syringe and vial package payloads with additional space for the avionics and respective subsystems. Overall, MULLET is a competitive airframe that balances each mission's performance to provide the greatest total score.

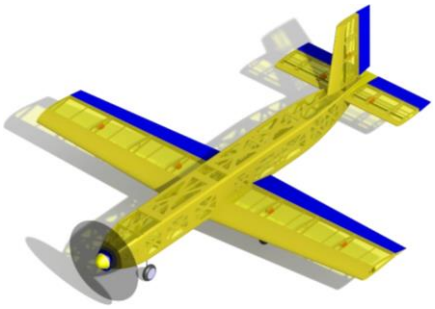

Figure 1-1: MULLET

Table 1-1: Demonstrated performance of MULLET

Parameter	M1	M2	M3	GM	Total
Gross Takeoff Weight [lb]	7.21	11.72	11.76	-	-
Takeoff Distance [ft]	8	18	16	-	-
Mission Time [s]	94	90	600	40	-
Cruise Airspeed [ft/s]	107.4	114.6	94.4	-	-
Number of Payloads	N/A	115 syringes	9 vial packages	-	-
Predicted Mission Score	1.00	1.78	2.90	0.38	6.06

2 Management Summary

The 2021–2022 ERAU DB team consisted of 40 students, ranging from freshmen to seniors, with a faculty advisor and six team leads to organize the sub-teams. Two positions worked directly under the Team Lead: the Chief Engineer and the Supply Chain Lead. Three teams worked under the Chief Engineer: Production Design, Manufacturing, and Flight Test. The Team Lead ensured the project remained on schedule, guided the leadership team to delegate tasks, and served as the team's main point of contact. The Chief Engineer directed and oversaw a senior design team consisting of a weights engineer, an aerodynamics engineer, a propulsion engineer, and a CAD engineer. The Chief Engineer also approved any necessary changes to the aircraft during the manufacturing process and analyzed the critical structures. The Supply Chain Lead was responsible for purchasing items and tracking the budget. The Production Design Lead created the CAD model of the aircraft and prepared files for 3D printing and laser cutting. The Manufacturing Lead led the largest sub-team in the fabrication and assembly of each aircraft and subsystem. The Flight Test Lead organized the testing and collection of data for the aircraft.

Figure 2-1 shows the described leadership structure. Additional team members worked under these leaders and participated in the production design, subsystem design, manufacturing, ground and flight test operations, and writing of the design report.

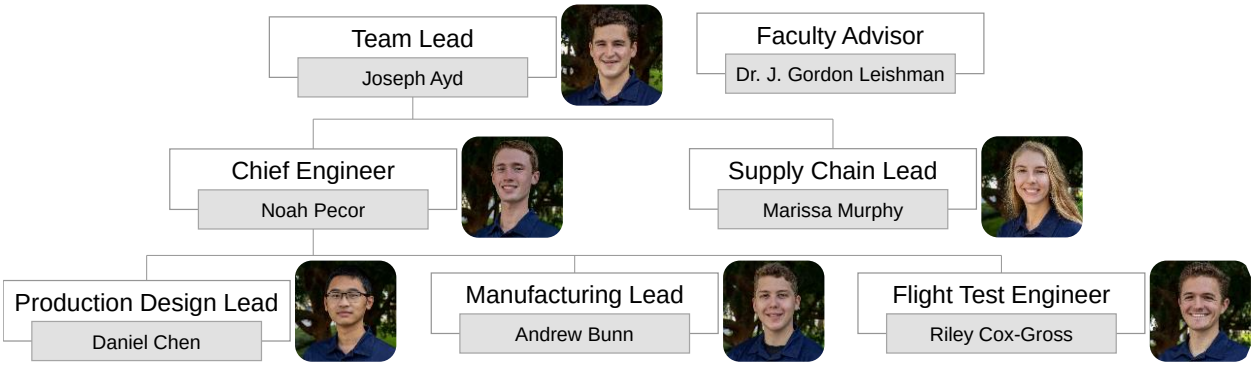

Figure 2-1: Management structure

2.1 Project Milestones

A schedule was defined at the start of the Fall 2021 semester that outlined the major events, milestones, and deliverables. The timeline was designed so that three iterations of the aircraft could be manufactured and tested before the competition fly-off, the third airframe being the competition iteration. The developed schedule allowed the teams to work in parallel, permitting flight test data to be acquired while the next aircraft iteration was being designed. The team worked throughout the year, meeting four times per week to work on the aircraft, with flight tests occurring on the weekends. The leadership team held weekly meetings to maintain consistent communication throughout the year. The Team Lead and Chief Engineer updated the faculty advisor on their progress weekly. Figure 2-2 shows the major timelines and milestones summarized in the form of a Gantt chart.

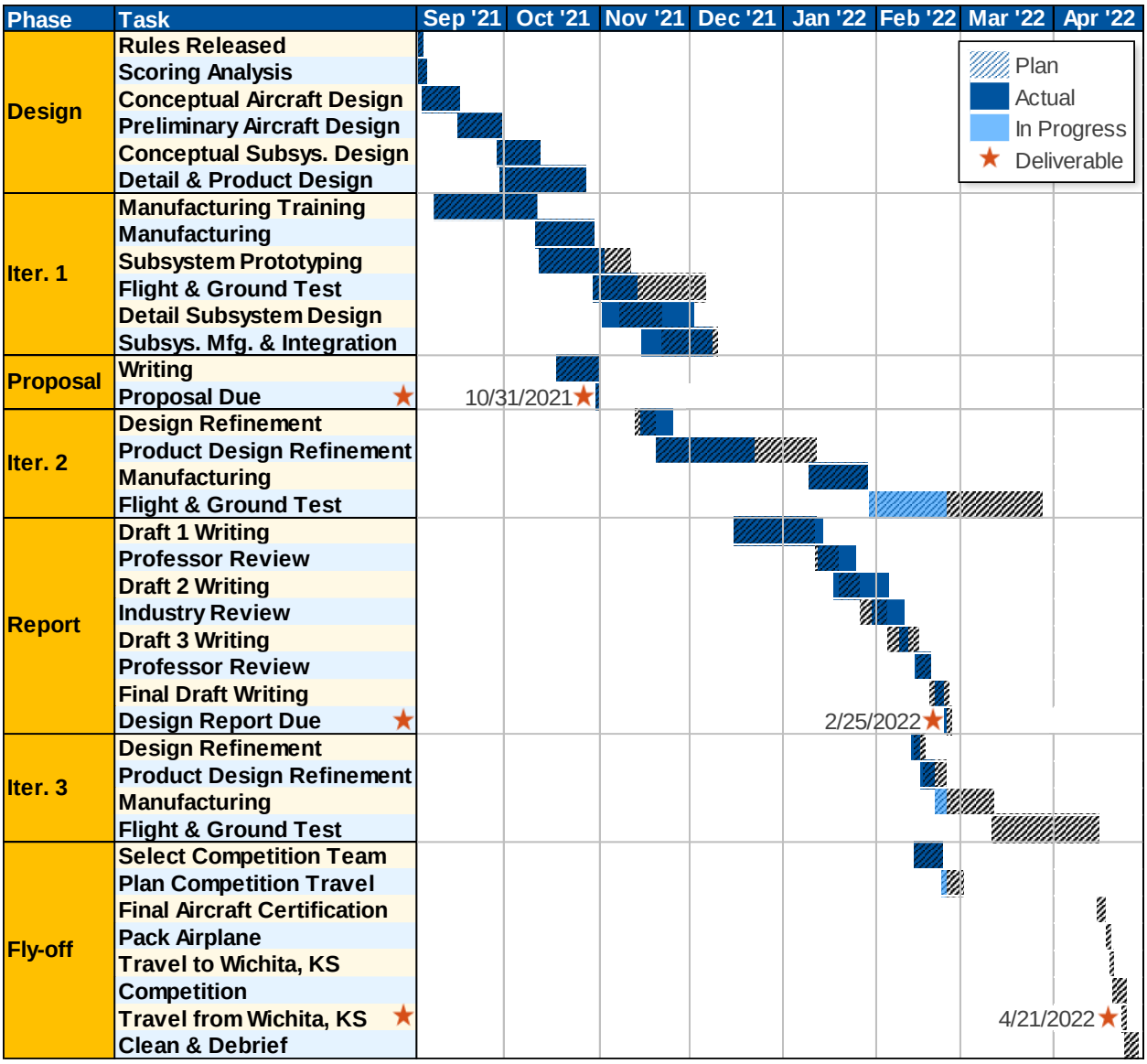

Figure 2-2: Project Gantt chart

3 Conceptual Design

The goal of the conceptual design phase was to select an aircraft configuration that maximized the mission scores. This process was accomplished by studying the mission requirements, performing a scoring analysis to create subsystem requirements, and using decision matrices to help select the aircraft and subsystem configurations.

3.1 Requirements

The primary requirements and limitations for the humanitarian UAV, in addition to the mission scoring equations, were specified by the AIAA DBF rules [1]. Table 3-1 shows the overall aircraft requirements that must be met during all missions. All flight missions were to be flown in the same course layout, shown in Figure 3-1.

Table 3-1: General aircraft requirements

#	Category	Requirement
AC-01	Configuration	Maximum linear dimension of the assembled aircraft is 8 ft
AC-02	Structures	Pass a wingtip load test with the maximum number of Mission 3 payloads declared and the heaviest battery installed
AC-03	Configuration	Fly all three missions in the same configuration, including all structure and deployment mechanisms (battery size may vary)
AC-04	Payload	Payload installation must be completed in less than 5 minutes
AC-05	Performance	Takeoff within 25 ft with all ground contact points starting forward of the start/finish line
AC-06	Configuration	No rotary wing or lighter-than-air configurations
AC-07	Propulsion	No form of externally assisted take-off
AC-08	Propulsion	Propeller driven and electric powered with an unmodified commercial brush or brushless electric motor
AC-09	Propulsion	Propeller or blades must be commercially produced
AC-10	Propulsion	Commercial ducted fan units are allowed
AC-11	Propulsion	Propeller diameter and/or pitch may be changed each flight attempt
AC-12	Propulsion	Propulsion power total stored energy cannot exceed 100 Wh
AC-13	Propulsion	Only one propulsion battery type; receiver battery is independent
AC-14	Propulsion	All commercial LiPo battery packs used must be identical
AC-15	Propulsion	Battery packs must be installed and secured with a minimum air gap of 0.25 in between it and any other battery pack
AC-16	Configuration	Maximum gross weight of 55 lb – set by the FAA [2]
AC-17	Performance	Service ceiling of 400 ft AGL – set by the FAA [2]
AC-18	Performance	Sustained, constant-altitude 2.25 g load factor turn – set by the team
AC-19	Structures	Removable wing and tail surfaces – set by the team

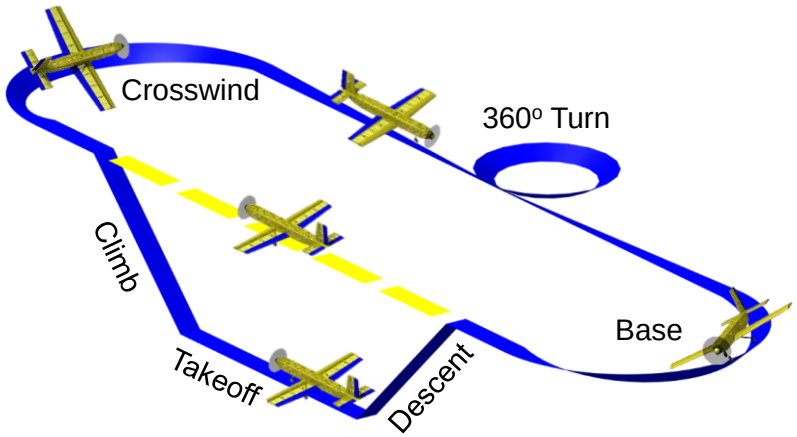

Figure 3-1: Mission lap

3.1.1 Mission 1

Mission 1 is a deployment flight that demonstrates the aircraft's basic flight capability. No payload is carried for this mission. The aircraft must complete three laps within the five-minute flight window and land successfully. One point is earned for the successful completion of this mission, as shown by Equation 3-1.

$$M1 = \begin{cases} 1, & \text{completion} \\ 0, & \text{failure} \end{cases} \tag{3-1}$$

3.1.2 Mission 2

Mission 2 is a staging flight for the transportation of vaccine syringes, shown in Figure 3-2. Scoring for this mission is determined by Equation 3-2, where the denominator is the maximum achieved by any team during the competition fly-off. Additional requirements for this mission are outlined in Table 3-2.

Payload volume:
7.50 ± 0.05 in^3
Weight:
0.041 ± 0.001 lb

Figure 3-2: Vaccine syringe payload (dimensions specified by team) [1]

$$M2 = 1 + \frac{(\#\ \text{syringes} \ / \ \text{time})_{\text{team}}}{(\#\ \text{syringes} \ / \ \text{time})_{\text{maximum}}} \tag{3-2}$$

Table 3-2: Mission 2 requirements

#	Category	Requirement
M2-01	Mission	The payload is 30 milliliter syringes, as shown in Figure 3-2
M2-02	Performance	Complete 3 laps within the 5-minute flight window (timed)
M2-03	Payload	Minimum number of syringes is 10

3.1.3 Mission 3

Mission 3 is a delivery flight for the transportation and deployment of vaccine vial packages, shown in Figure 3-3. Scoring for this mission is expressed by Equation 3-3, where the denominator is the maximum achieved by any team during the competition fly-off. Additional requirements for this mission are outlined in Table 3-3. In summary, the aircraft must land and deliver one vial package after each flight lap, deploying as many vial packages as possible within the 10-minute flight window.

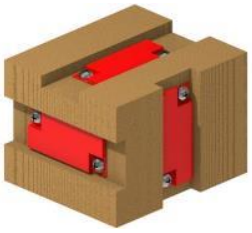

Dimensions:
2.50 x 3.00 x 3.50 ± 0.13 in
Weight:
0.50 ± 0.01 lb

Figure 3-3: Vaccine vial package payload [1]

$$M3 = 2 + \frac{(\#\ \text{successful deployments})_{\text{team}}}{(\#\ \text{successful deployments})_{\text{maximum}}} \quad (3\text{-}3)$$

Table 3-3: Mission 3 requirements

#	Category	Requirement
M3-01	Mission	The payload is vaccine vial packages, as shown in Figure 3-3
M3-02	Payload	Minimum number of vial packages is 1
M3-03	Payload	Maximum number of vial packages is the lesser of the maximum declared during technical inspection, or the maximum number of syringes flown during Mission 2, divided by 10 and rounded down to the nearest whole number
M3-04	Mission	After each flight lap, land and taxi to the designated payload drop area to remotely deploy one vial package (the drop area is between 25 ft prior to the start/finish line and the start/finish line itself)
M3-05	Mission	After dropping one vial package, taxi past the start/finish line and stop prior to takeoff for the next lap
M3-06	Mission	Remotely deploy as many vial packages as possible within the 10-minute flight window
M3-07	Mission	Vial packages must not exceed a 25 g load factor at anytime
M3-08	Mission	The mission is complete after the final vial package is deployed and the aircraft has crossed the start/finish line, or the 10-minute flight window expires

3.1.4 Ground Mission

The Ground Mission is an operational demonstration of the ability to prepare the aircraft for flight in a timely manner. Scoring for this mission is expressed by Equation 3-4, where the numerator is the minimum achieved by any team during the competition fly-off. Additional requirements for this mission are outlined in Table 3-4.

$$GM = \frac{(\text{time})_{\text{minimum}}}{(\text{time})_{\text{team}}} \quad (3\text{-}4)$$

Table 3-4: Ground Mission requirements

#	Category	Requirement
GM-01	Mission	Mission box is 10 ft by 10 ft
GM-02	Mission	Only the assembly crew member can touch the aircraft and payloads during the Ground Mission
GM-03	Mission	First, load the full Mission 2 payload while timed
GM-04	Mission	Second, unload the full Mission 2 payload while timed
GM-05	Mission	Third, load the full Mission 3 payload while timed
GM-06	Mission	Fourth, remotely deploy the full Mission 3 payload one at a time to validate its functional performance (not timed)

The combined team fly-off score is the sum of the mission scores (with a maximum of seven). Teams are then ranked by their combined fly-off score multiplied by their report score (with a maximum of 100%).

3.2 Scoring Analysis

The first step in the design process was to perform a scoring analysis to determine the best payload for MULLET. To maximize the mission scores most effectively, certain parameters of the aircraft's design were studied to determine the optimal payload configuration.

First, the Mission 2 score, as given by Equation 3-2, was plotted. By analyzing the performance of winning DBF teams over the past three years, it was determined that the best team would likely complete three laps carrying 130 syringes in 80 seconds. By selecting various numbers of syringes and flight times for the aircraft, the Mission 2 score could be obtained; this relationship is plotted in Figure 3-4.

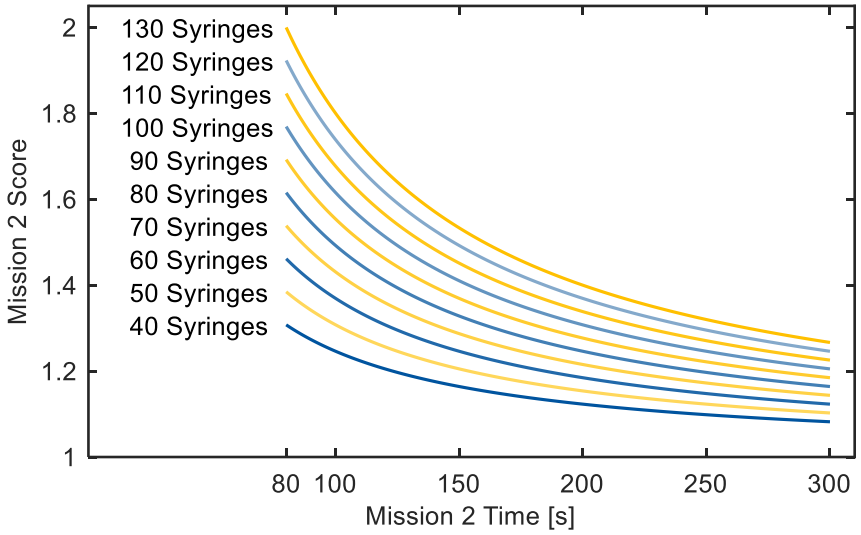

Figure 3-4: Mission 2 scoring analysis

Figure 3-4 shows that a decrease in mission time does not yield a comparable improvement to the Mission 2 score obtained with an increase in the number of syringes carried. To validate this finding, an energy cost-benefit analysis, shown in Table 3-5, was performed to evaluate the effect of changing parameters on the available propulsion energy (limited by Requirement AC-12).

Table 3-5: Mission 2 energy cost-benefit analysis

Parameter	Cost	Benefit
Linear increase in number of syringes	A linear increase in weight and therefore a *linear increase in energy consumption*	Linear score increase
Linear decrease in mission time	A linear increase in flight speed resulting in a quadratic increase in drag and therefore a *quadratic increase in energy consumption*	Linear score increase

The energy cost of increasing the number of syringes was found to be lower than the cost of decreasing the mission flight time, which validates the finding shown in Figure 3-4. Therefore, it was determined that the number of syringes should be optimized over the mission time to maximize the Mission 2 score. For initial design purposes, 110 syringes were selected as the optimal Mission 2 payload because this payload would have a comparable volume to historical DBF aircraft.

The Mission 3 score depends solely on the number of vaccine vial packages that are successfully deployed. Therefore, the number of vial packages deployed within the 10-minute flight window was maximized. To accomplish this goal, historical lap times were gathered for winning DBF aircraft of comparable missions over the past three years. A correction factor was applied to the historical lap time to account for the time of takeoff, landing, and vial package deployment during each lap. It was then determined that the minimum achievable lap time for Mission 3 was 60 seconds, indicating that a maximum of 10 vial packages would be deployed by any team at the competition fly-off. However, this time is highly unlikely to be achieved as the average cruise airspeed required (130 ft/s) is greater than all but one historical aircraft considered. Therefore, nine vaccine vial packages were selected as the optimal Mission 3 payload. During the preliminary design, the payload volume and aircraft lifting capability would need to be optimized to ensure the airspeed required to deliver all vial packages is achieved while balancing the overall propulsion system performance. Table 3-6 summarizes the payload selections obtained from the scoring analysis.

Table 3-6: Initial payload selections

Mission	Number of Payloads	Weight [lb]	Volume [in^3]
M2	110 syringes	4.51	825
M3	9 vial packages	4.56	237

3.3 Aircraft Configuration

As a result of the scoring analysis, and to meet the mission objectives, the following parameters were selected as key factors in the design: endurance, speed, payload volume, and wing lift. To determine the best design possible, three configurations were considered, shown in Figure 3-5. According to initial propulsion estimates, a single motor configuration was necessary to balance Requirements AC-05 and AC-12. It was determined that a tractor configuration was necessary for the motor to clear the deployed payload per Requirement M3-04.

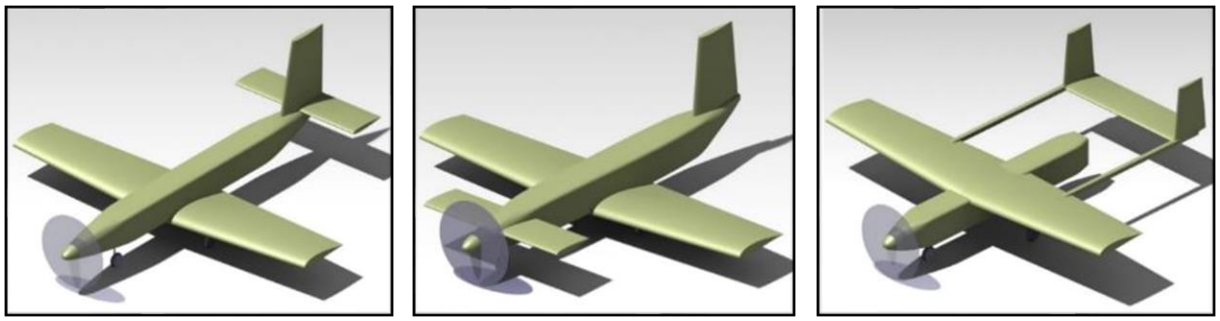

Figure 3-5: Considered aircraft configurations: conventional, control-canard, and twin-boom (left to right)

3.3.1 Conventional, Low-Wing, Single-Engine Tractor

The first configuration considered was a conventional, low-wing, single-engine tractor. The primary benefits of this design were the ease of access to the internal subsystems and the ability to load and unload the payload through the top of the fuselage. The low-wing configuration accommodated a shorter, wider landing

gear to decrease drag and improve ground handling characteristics. Ground handling was critical for Mission 3 to maneuver for vial package deployment in the payload zone as well as stopping for takeoff at the start/finish line per Requirements M3-04 and M3-05. An additional benefit of this configuration was the ease of manufacturing of the horizontal and vertical tails because of their ability to attach to a single load-carrying member.

One disadvantage of this configuration was the manufacturing complexity of the wing carry-through because of the required dihedral for lateral stability on a low-wing aircraft. Additionally, the takeoff rotation angle was inherently limited by the fuselage being lengthened to increase the internal payload volume, which limited the achievable angle of attack for the wing during takeoff.

3.3.2 Control-Canard, Low-Wing, Single-Engine Tractor

The next configuration considered was a control-canard, low-wing, single-engine tractor. This layout was like the conventional low-wing configuration in that the fuselage and wing shared the same general geometry. One benefit of the canard layout over the conventional layout was the decrease in required wing lift coefficient because the canard produced positive lift for longitudinal stability, assisting in meeting Requirement AC-05, while a horizontal tail produced downforce.

However, the canard presented more drawbacks compared to the conventional layout, primarily regarding weight and flight qualities. First, more structure was required to support surfaces in both the fore and aft positions on the fuselage compared to surfaces in only the aft position. Consequently, the structure for the canard carry-through interfered with the proposed battery location in the nose of the fuselage. Access to the forward payload bay was also limited because of the increased structure present for the canard and batteries. Second, the longitudinal stability of the aircraft was a concern because most of the canard was in the slipstream of the propeller due to a single-engine tractor configuration being the only practical option to deploy payloads while taxiing. This issue was further complicated by the canard's need to stall before the wing to avoid adverse stall characteristics.

3.3.3 Twin-Boom, High-Wing, U-Tail, Single-Engine Tractor

The final configuration considered was a twin-boom, high-wing, single-engine tractor with a U-tail. In this layout, a high wing was selected to allow the booms and tail to achieve a greater takeoff rotation angle and to clear the deployed Mission 3 payloads while taxiing. The primary benefit of this layout was the ability to open the aft fuselage wall for payload deployment. Additionally, the use of carbon fiber booms improved the ease of manufacturing of the primary aircraft structure. Another benefit was the decreased fuselage length, which reduced the total wetted area of the aircraft thereby decreasing the overall drag. The decreased drag would assist in achieving a greater cruise airspeed, improving the ability to deploy nine vial packages during Mission 3.

The main downside of the twin-boom layout was the restricted access to the payload bay with the wing carry-through being on the top of the fuselage, likely increasing the complexity of any payload subsystems. Although dihedral was not necessary for lateral stability for the high-wing design, which would allow a single spar to easily carry through both wings, the twin-boom structure significantly complicated the ability to

design removable wing and tail surfaces for transport per Requirement AC-19. Additionally, the wetted area from the twin-booms and the low-pressure zone behind the fuselage would increase drag, possibly negating any improvements from the decrease in fuselage wetted area. Twin-booms would also increase the structural weight going to the tail, which would negatively affect both the takeoff and flight performance. Finally, the main landing gear design necessitated a tradeoff between ground handling and drag. If placed low on the fuselage, it would be shorter (less drag) but narrow (poor ground handling). Alternatively, if placed high on the wings, it would be longer (more drag) but wide (good ground handling).

3.3.4 Selected Configuration

Decision matrices were used to assist in selecting the aircraft configuration and other layout decisions. The steps of the decision matrix process are shown in Table 3-7.

Table 3-7: Decision matrix process

#	Step
1	Established decision matrices for design decisions not otherwise governed by a method of analysis
2	Selected criteria as being important to consider for each decision matrix
3	Weighted each criterion based on its impact on the requirements, from 1 (least) to 3 (greatest)
4	Divided each weighting by the total of all weightings to obtain the percentage ratio for each criterion
5	Graded each combination of criterion and design option, from 1 (worst) to 5 (best)
6	Calculated the weighted total for each design option by multiplying the option's rating for each criterion by the respective criterion's weighting

The first decision matrix selected one of the previously discussed aircraft configurations. In total, 11 criteria were considered with weight and takeoff performance being the most significant per Requirements AC-05, AC-12, M2-02, and M3-06. This decision matrix is shown in Table 3-8, where the conventional configuration obtained the highest score and, therefore, was selected as the competition configuration.

Table 3-8: Configuration decision matrix

Criteria	Weight		Conventional	Canard	Twin Boom
Weight	3	16.7%	5	4	3
Takeoff Performance	3	16.7%	4	5	4
Payload Loading	2	11.1%	5	4	4
Payload Storage	2	11.1%	5	4	4
Payload Dropping	2	11.1%	4	4	5
CG Flexibility	2	11.1%	5	3	5
Stability & Control	1	5.6%	5	3	5
Drag	1	5.6%	5	5	4
Motor Placement	1	5.6%	5	1	5
Manufacturing	1	5.6%	5	5	4
Weighted Total	**18**	**100.0%**	**4.72**	**3.94**	**4.17**

3.3.5 Layout of Selected Configuration

First, the best payload loading direction needed to be determined between rear, top, or side loading; front loading was not considered because of the placement of the motor. A decision matrix was created with the following criteria: weight, structural feasibility, payload loading time, and payload loading ease. Top payload loading significantly outweighed both rear and side loading; this decision matrix is omitted for brevity.

With top loading on a conventional configuration in mind, the wing placement of low, mid, or high was determined next. This decision matrix is given in Table 3-9, from which a low wing was selected.

Table 3-9: Wing placement decision matrix

Criteria	Weight		Low	Mid	High
Weight	3	21.4%	5	4	4
Takeoff Performance	3	21.4%	5	4	4
Ground Handling	2	14.3%	5	4	4
Payload Loading	2	14.3%	5	2	3
Stability	1	7.1%	3	4	5
Payload Storage	1	7.1%	5	1	5
Manufacturing	1	7.1%	5	3	5
Structural Design	1	7.1%	4	3	5
Weighted Total	**14**	**100.0%**	**4.79**	**3.36**	**4.14**

Next, the horizontal tail placement of conventional (low), cruciform (mid), or T-tail (high) was determined. This decision matrix is given in Table 3-10, in which a conventional tail was selected.

Table 3-10: Horizontal tail placement decision matrix

Criteria	Weight		Conventional	Cruciform	T-tail
Weight	3	33.3%	5	3	2
Structural Design	2	33.3%	5	3	2
Downwash	2	22.2%	3	4	5
High Alpha Effect on HT	1	11.1%	5	3	2
High Alpha Effect on VT	1	11.1%	4	5	5
Weighted Total	**9**	**100.0%**	**4.44**	**3.44**	**3.00**

Lastly, the landing gear layout was determined. In accordance with Requirement M3-04, the landing gear must clear the deployed payload and provide ample ground handling; therefore, a tricycle landing gear configuration was selected.

3.4 Staging and Delivery Mechanisms

MULLET contained two subsystems: a vaccine syringe staging mechanism (VSSM) for Mission 2 and a vaccine vial package delivery mechanism (VVPDM) for Mission 3. These subsystems, while independent,

must be integrated in a way that balanced the weight, payload volume, loading and unloading time, and other criteria. Decision matrices, as explained in Section 3.3.4, were used to select the best subsystem concepts.

3.4.1 Selected Vaccine Syringe Staging Mechanism

The VSSM was required to store the syringes in the highest density possible while decreasing the loading and unloading times. This approach maximized the number of syringes that could be carried within the available payload volume, increasing the Mission 2 score and maximizing the Ground Mission score. The concepts considered for the VSSM are shown in the decision matrix in Table 3-11. Ultimately, fabric bags were selected because of their low weight, fast loading and unloading times, and low stowage volume.

Table 3-11: VSSM decision matrix

Criteria	Weight		Storage Trays	Folding Box	Fabric Bags	Loose in Fuselage
Weight	3	21.4%	3	2	4	5
Load Time	3	21.4%	2	4	4	5
Unload Time	3	21.4%	2	4	5	1
Stowage Volume	2	14.3%	2	3	4	5
Ease of Use	2	14.3%	3	1	4	5
Manufacturing	1	7.1%	4	2	4	5
Weighted Total	**14**	**100.0%**	**2.50**	**2.86**	**4.21**	**4.14**

3.4.2 Selected Vaccine Vial Package Delivery Mechanism

The VVPDM must store nine vaccine vial packages (the Mission 3 payload selected in Section 3.2), move them inside the payload bay for deployment while maintaining a stable center of gravity, and safely deliver them to the ground per Requirement M3-07. The primary concepts considered for the VVPDM included a conveyor belt or auger for storing/moving the vial packages and a door slide, elevator, or arm and claw to deploy the vial packages. To clarify, the purpose of the auger concept was for a rotating spring to store and move vial packages in Mission 3 and then compress to free-up payload volume for Mission 2. These basic concepts are illustrated in Figure 3-6.

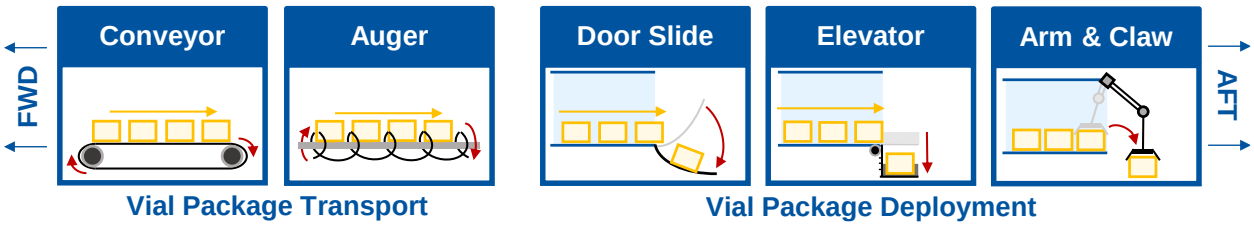

Figure 3-6: Basic VVPDM concepts considered

The two transport and three deployment concepts were combined into four final VVPDM options, as shown in the decision matrix in Table 3-12. Ultimately, the configuration of a one-level conveyor belt to a door slide

was selected because it would be lightweight, easy to manufacture, and would balance the required payload volume against the vial package deployment time.

Table 3-12: VVPDM decision matrix

Criteria	Weight		Conveyor to Elevator or Arm & Claw	Auger to Door Slide	2-Level Conveyor to Door Slide	1-Level Conveyor to Door Slide
Weight	3	25.0%	1	3	3	5
Volume	3	25.0%	3	5	2	4
Deploy. Time	2	16.7%	2	2	4	5
Load Time	2	16.7%	2	3	3	5
Manufacturing	1	8.3%	1	2	3	5
Part Count	1	8.3%	1	2	3	5
Weighted Total	**12**	**100.0%**	**1.83**	**3.17**	**2.92**	**4.75**

4 Preliminary Design

Following the conceptual design phase during which the conventional, low-wing, single-engine tractor was selected, the preliminary design phase aimed to maximize the mission scores through sizing analyses.

4.1 Methodology and Trade Studies

Initial sizing analyses were completed by iterating the gross weight, wing area, takeoff performance, and propulsion system. By combining historical weight fractions with the payloads selected in Section 3.2, an estimate for the initial aircraft weight was obtained and validated by historical mass properties of component weights. Next, the wing area was defined to meet the primary constraint (takeoff distance) per Requirement AC-05. Then, a takeoff analysis using Gudmundsson's method [3] to solve for airspeed and required thrust validated that the takeoff performance requirement was met. Finally, a propulsion analysis was conducted using eCalc [4] to select a motor and battery. An iterative mission segment approximation was used to validate that the takeoff and cruise endurance requirements were met with the selected propulsion system. The previous steps, further explained in Figure 4-1, were iterated until the initial aircraft configuration and sizing met all the design requirements.

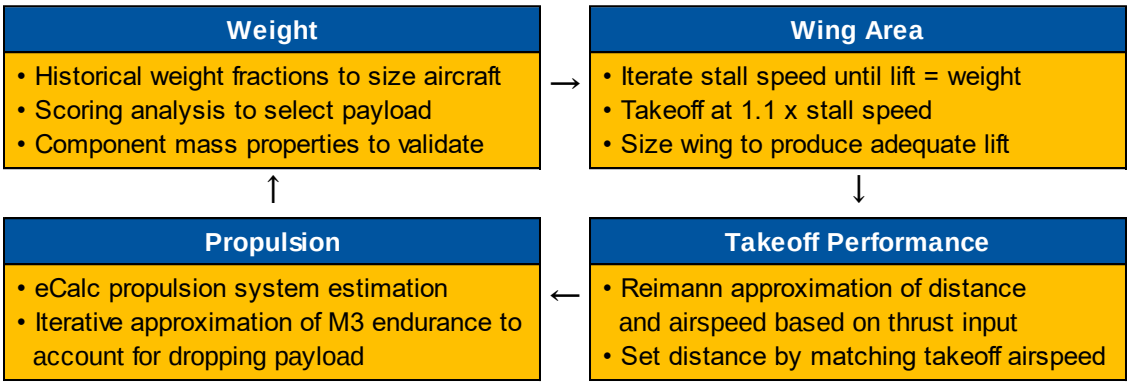

Figure 4-1: Iterative preliminary design sizing methodology

4.2 Weight

The initial aircraft weight estimation began by collecting statistics from historical data on comparable aircraft, organized in Table 4-1. It is important to note that the historical aircraft considered were designed for different missions, which inherently changed the takeoff weight, payload weight, and empty weight. However, the weight fractions provided a good starting point for the design.

Table 4-1: Weights of historical DBF aircraft

Parameter	ERAU DB 2020 [5]	USC 2020 [5]	Georgia Tech 2020 [5]	ERAU DB 2021 [6]	Average
Configuration	Twin-Engine Twin-Boom	Single-Engine Conventional	Single-Engine Conventional	Twin-Engine Conventional	**N/A**
W_0 [lb]	12.02	19.43	20.60	27.00	**19.76**
W_b / W_0	0.14	0.14	0.09	0.09	**0.11**
W_e / W_0	0.55	0.33	0.21	0.47	**0.39**
W_p / W_0	0.31	0.54	0.69	0.45	**0.50**

Additional weight considerations were driven by the scoring analysis explained in Section 3.2, where a target payload of 110 syringes (weight of 4.51 lb) and nine vial packages (weight of 4.56 lb) were selected for Missions 2 and 3, respectively. Next, Equation 4-1, modified from Raymer [7] to include battery weight (1.55 lb) as a known constant, was used to solve for the initial design takeoff weight using a historical battery fraction of 0.11 and a historical empty weight fraction of 0.39.

$$W_0 = \frac{W_b + W_p}{1 - \left(\frac{W_b}{W_0}\right) - \left(\frac{W_e}{W_0}\right)} \tag{4-1}$$

This process resulted in an initial design takeoff weight of 12.21 lb. Then, subtracting the battery and payload weights resulted in an empty aircraft weight of 6.11 lb. Early mass property iterations indicated that the empty weight of the aircraft would need to be increased to 6.80 lb. However, further iterations of the takeoff analysis, paired with initial propulsion estimates, indicated that the greatest allowable empty weight to meet Requirements AC-05 and M3-06 was 6.60 lb. As explained subsequently in Section 4.5, it was apparent that the propulsion system would not support the deployment of nine vial packages in Mission 3.

To obtain an empty weight of 6.60 lb, the payload selection and empty weight fraction were adjusted. Ultimately, the payload was reduced to 105 syringes (4.31 lb) and eight vial packages (4.05 lb) for Missions 2 and 3, respectively, shown in Table 4-2. The empty weight fraction was iterated upon until a design takeoff weight of 12.46 lb was obtained, resulting in an empty weight of 6.60 lb.

Table 4-2: Refined payload selections

Mission	Number of Payloads	Weight [lb]	Volume [in^3]
M2	105 syringes	4.31	788
M3	8 vial packages	4.05	210

4.3 External Geometry

4.3.1 Wing

Requirement AC-05 was the primary constraint to the wing sizing. First, a mission segment lift coefficient analysis, summarized in Table 4-3, was performed using the initial weight estimate from Section 4.2 and the takeoff and cruise airspeeds explained later in Section 4.5.

Table 4-3: Mission segment lift coefficient summary: clean (no flaps) unless specified

Mission Segment		*n* [g]	*W* [lb]	*v* [ft/s]	*Re*	Req'd C_L (Aircraft) $= \frac{2nW}{\rho v^2 S_W}$	Req'd C_L (Wing) $= \frac{C_{L\text{-aircraft}}}{0.90}$	Req'd C_l (Airfoil) $= \frac{C_{L\text{-wing}}}{0.90}$
M1	**Takeoff – dirty**	1	8.15	33.4	2.35×10^5	0.93	1.03	1.15
	Cruise	1	8.15	90.0	6.33×10^5	0.13	0.14	0.16
M2	**Takeoff – dirty**	1	12.46	33.4	2.35×10^5	1.42	1.58	1.76
	Cruise	1	12.46	90.0	6.33×10^5	0.20	0.22	0.24
	Turns	2.25	12.46	60.0	4.22×10^5	0.99	1.10	1.22
M3	**Takeoff – dirty**	1	12.20	33.4	2.35×10^5	1.39	1.55	1.72
	Start cruise	1	12.20	92.4	6.50×10^5	0.18	0.20	0.22
	Start turns	2.25	12.20	60.0	4.22×10^5	0.97	1.08	1.20
	End cruise	1	8.15	92.4	6.50×10^5	0.12	0.13	0.15
	End turns	2.25	8.15	60.0	4.22×10^5	0.65	0.72	0.80

The maximum lift coefficient required for the airfoil (takeoff during Missions 2 and 3) revealed that flaps would be necessary. Various airfoils, shown in Table 4-4, were considered to achieve the lift coefficient required from Table 4-3. Low Reynolds number airfoils were heavily studied for MULLET's flight regime.

Table 4-4: Considered wing airfoils (Re_{cruise} = 500,000) [8], [9], [10]

Airfoil	*t/c*	Max Camber [%c]	$C_{l\text{-}max}$	α_{stall} [deg]	$C_{d\text{-}min}$	Notes
Clark Y	0.12 at 0.28 *x/c*	3.4	1.43	12	0.007	Flat lower surface for mfg.
SD7062	0.14 at 0.26 *x/c*	3.5	1.63	15	0.010	Low Re, high lift
MH 84	0.14 at 0.22 *x/c*	4.1	1.70	12	0.010	High lift

The SD7062 airfoil was subsequently selected because of its desirable low Reynolds number characteristics. Table 4-5 summarizes additional design parameters obtained from Selig [11] (the airfoil designer) and other experimental data.

Table 4-5: SD7062 experimental data comparison to selected design values

Parameter	Selig [11]	Experimental [10]	Experimental [9]	Design Value
$C_{l\text{-}max}$	1.63	1.55	N/A	1.63
$C_{m\text{-}c/4}$	-0.95	N/A	N/A	-0.095
α_{0L} [deg]	-4.2	-3.7	N/A	-3.5
$C_{l\alpha}$ [/deg]	0.120	0.095	0.107	0.115
$C_{m\alpha}$ [/deg]	0.00043	N/A	N/A	0.0043
$\Delta C_{l\text{-}wf}$ (30%c flaps, 15 deg deflection)	N/A	N/A	0.55	0.52 Calculated using Datcom [12]

Next, the wing was sized to achieve the maximum required wing overall lift coefficient of 1.58 (Table 4-3). By applying a generalized uncertainty factor of 11% to the SD7062 2D lift coefficient of 1.62 to allow a margin for the actual performance to be lower than expected, a 2D lift coefficient of 1.45 was used for the design. Then, by applying correction factors from Equation 9-71 of Gudmundsson [3] and Chapter 6.1.4.1 of Datcom [12], the 3D lift coefficient was then determined to be 1.29; this value was greater than that required for any clean mission segment (Table 4-3).

As previously mentioned, flaps would be required to achieve the takeoff lift coefficient. Spanwise flaps, including flaps and flaperons over the entire exposed area of the wing, were selected to achieve the greatest possible lift coefficient. The chordwise flap percentage and required flap deflection to achieve this lift were iterated until both takeoff performance and propulsion sizing met the design requirements. Ultimately, 30% chord flaps with a deflection of 15 degrees was obtained. By applying the methods from Chapters 6.1.1.3 and 6.1.4.3, respectively, from Datcom [12], the 2D change in lift coefficient with flaps was calculated to be 0.52 and the 3D change to be 0.43. Finally, by adding the 3D change in lift coefficient with flaps to the 3D lift coefficient without flaps, the maximum lift coefficient was determined to be 1.72; this value is greater than that required for any dirty mission segment, except for the Mission 2 takeoff (Table 4-3). The small difference between the required Mission 2 takeoff lift coefficient and the lift coefficient produced by the SD7062 airfoil with flaps was deemed acceptable because of the uncertainty margins applied to the original calculations. Therefore, the wing design was expected to meet the requirements.

With an established lift coefficient, the lift could then be set equal to the weight to solve for the required wing area for takeoff using Equation 4-2.

$$C_L = \frac{L}{QS_W} = \frac{nW}{QS_W} = \frac{2nW}{\rho v^2 S_W} \rightarrow S_W = \frac{2nW}{\rho v^2 C_L} \tag{4-2}$$

The required wing area was calculated to be 6.90 ft^2. Next, the remaining wing geometry was determined. The aspect ratio, taper ratio, twist, dihedral, and chord location of the zero-sweep angle were defined using historical averages of similar DBF aircraft, vortex lattice methods, and consideration of manufacturability. The final wing geometry is described in Table 4-6.

Table 4-6: Wing geometry

Parameter	Value	Methodology
Aspect Ratio	5.1	Historical average, increased for a reduction in induced drag
Taper Ratio	0.7	Historical average, decreased to improve spanwise efficiency factor
***x/c* at Zero-Sweep**	0.25	To place wing spar at SD7062's aerodynamic center and maximum *t/c*
Twist [deg]	0	Difficult to manufacture symmetric balsa-built-up wings with twist
Dihedral [deg]	3	Necessary for stability in low-wing configuration [13]
Area [ft^2]	6.90	Calculated as explained previously
Span [ft]	5.93	Calculated from aspect ratio and area
Root Chord [in]	16.42	Calculated from taper ratio, aspect ratio, and span
Tip Chord [in]	11.49	Calculated from taper ratio and root chord

Finally, the ailerons were sized. For ease of manufacturing, the ailerons would use the previously determined flap chord ratio of 30%. The remaining parameter to be determined was the control surface span, for which a historical average flap span to exposed wingspan ratio of 40% was used. This resulted in a flap span of 13.3 in and an aileron span of 19.5 in.

4.3.2 Empennage

The tail surfaces were sized by selecting an airfoil, obtaining historical sizing parameters, and calculating the moment arm for an adequate tail volume coefficient. Table 4-7 includes the considered tail airfoils, from which the NACA-0012 was selected for both the horizontal and vertical tail to allow adequate thickness to fit the control surface servos.

Table 4-7: Considered tail airfoils (Re_{cruise} = 500,000) [8]

Airfoil	*t/c*	$C_{l\text{-}max}$	α_{stall} [deg]	$C_{d\text{-}min}$	Notes
NACA-0010	0.10 at 0.30 *x/c*	1.20	13	0.006	Less drag than 0012
NACA-0012	0.12 at 0.30 *x/c*	1.23	14	0.008	Historically popular
SD8020-010-88	0.10 at 0.28 *x/c*	1.10	12	0.006	Low Re

Tables 4-8 and 4-9 summarize tail parameters of previous DBF aircraft with similar configurations and size.

Table 4-8: Horizontal tail sizing parameters of historical DBF aircraft

Parameter	ERAU DB 2020 [5]	USC 2020 [5]	Georgia Tech 2020 [5]	ERAU DB 2021 [6]	Average
S_{HT}/S_W Ratio	0.24	0.18	0.15	0.38	**0.24**
Aspect Ratio	3.32	4.43	2.22	4.00	**3.50**
Taper Ratio	1.00	1.00	1.00	1.00	**1.00**

Table 4-9: Vertical tail sizing parameters of historical DBF aircraft

Parameter	ERAU DB 2020 [5]	USC 2020 [5]	Georgia Tech 2020 [5]	ERAU DB 2021 [6]	Average
S_{VT}/S_W Ratio	0.11	0.10	0.07	0.19	**0.11**
Aspect Ratio	1.53	1.92	1.00	1.17	**1.40**
Taper Ratio	1.00	1.00	1.00	1.00	**1.00**

The horizontal tail area was initially sized using historical averages of the area, aspect, and taper ratios. Per Greiner [13], an aspect ratio of 3.5 was acceptable for a low Reynolds number airfoil. A taper ratio of 1.0 was also sufficient for the benefit of manufacturability with no adverse aerodynamic effects at low Reynolds numbers. The horizontal tail area was calculated to be 1.66 ft^2 using the horizontal tail to wing area ratio of 24%. The span and chord length could then be calculated using the aspect and taper ratios; these dimensions are presented later in Section 5.1.

Like the horizontal tail, the vertical tail was initially sized using the area ratio. However, the directional stability of past ERAU DB aircraft was insufficient, requiring design changes in later aircraft iterations. Because two of the four aircraft in the statistical database were past ERAU DB entries, the vertical tail to wing area ratio was increased to 14%, yielding a vertical tail area of 0.97 ft^2. The vertical tail's aspect ratio of 1.4 was within the range recommended by Greiner [13]. The vertical tail's taper ratio was reduced to 0.75 for visual appeal with no adverse aerodynamic effects at low Reynolds numbers. All remaining dimensions are given later in Section 5.1.

To determine the required tail moment arms, *L*, the tail volume coefficients, *V*, were obtained from similar aircraft types, as shown in Table 4-10.

Table 4-10: MULLET and typical tail volume coefficients [7]

Airplane Type	$\bar{V}_{HT} = \frac{S_{HT}L_{HT}}{S_W \bar{C}_W}$	$\bar{V}_{VT} = \frac{S_{VT}L_{VT}}{S_W b_W}$
Sailplane	0.50	0.02
Single-Engine General Aviation	0.70	0.04
Twin-Engine General Aviation	0.80	0.07
Military Cargo/Bomber	1.00	0.08
MULLET	**0.58**	**0.065**

By solving for the moment arm from the tail volume terms selected for MULLET, the aerodynamic centers of the horizontal and vertical tails were placed at 35.92 in and 35.07 in from the CG, respectively.

Finally, the elevators and rudder were sized. A historical chord ratio of 30% was selected for the elevator. The elevator chord line was projected onto the vertical tail to size the rudder, resulting in an effective rudder chord ratio of slightly greater than 30% (above the historical average). Both the moment arm and control surface selections were validated by the stability and control analysis presented in Section 4.6.

4.3.3 Fuselage

Using the refined payload selections as shown in Table 4-2, the required payload volume was determined to be 788 in^3. The fuselage was initially sized to have cross-sectional dimensions of 6 in by 6 in. With bulkheads measuring 0.5 in thick, the internal payload bay cross-sectional area was 5 in by 5 in (25 in^2). To accommodate the required Mission 2 payload volume of 788 in^3, a payload bay length of 36 in was selected. This length granted a 14% margin over the required payload volume to account for miscellaneous payload bay volume occupied by structures such as the VVPDM and the wing box. Lastly, the nose and tail portions of the fuselage were contoured based on best aerodynamic practices recommended by Greiner [13].

4.3.4 Landing Gear

The main and nose gear were located on the aircraft using a method explained in Chapter 11.2 of Raymer [7]. Raymer recommended a tail-strike angle of 10 to 15 degrees, a tipback angle of greater than 15 degrees, an overturn angle of less than 63 degrees, and a nosewheel supporting 8% to 15% of the aircraft's weight. First, the main gear was placed at FS 33.85 in, allowing for a tail-strike angle of 14.94 degrees and a tipback angle of 16.49 degrees. Second, the nose gear was placed at FS 15.86 in so that it supported 9.5% of the aircraft's weight. Finally, the main gear was placed at BL 8.50 in, such that the overturn angle was 35.62 degrees. This landing gear layout, shown in Figure 4-2, assisted in meeting Requirements AC-05 and M3-04.

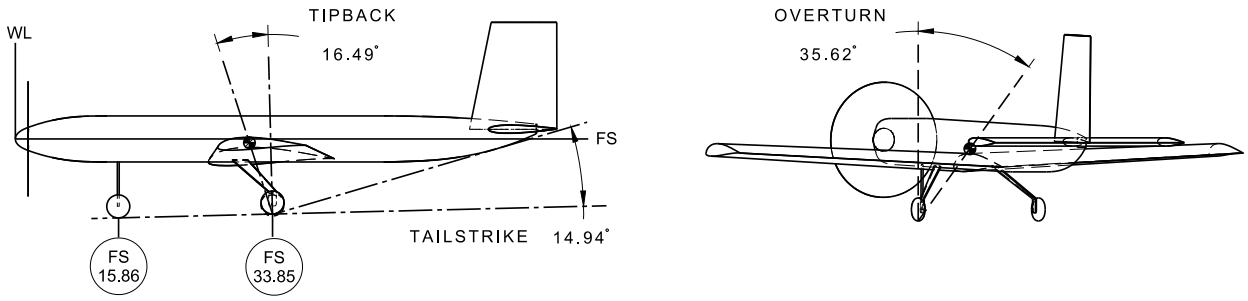

Figure 4-2: Landing gear geometry

4.4 Drag

The drag of MULLET was analyzed using a drag build-up method from Chapter 15 of Gudmundsson [3]. In this method, the contributions of the skin friction and pressure drag of each component, miscellaneous effects, and the lift-induced drag were considered. The components used included the wings, horizontal tail, vertical tail, and fuselage. The skin friction coefficient was combined with the pressure drag and was corrected for interference and geometry. Equation 4-3 was used to calculate the minimum drag, where C_{Df} is the skin friction coefficient, *FF* is a form factor, *IF* is the interference factor, and S_{wet} is the wetted area for each component of the aircraft. Skin friction and pressure drag are accounted for in the same term (C_{Df}).

$$C_{D_{min}} = \left[\left(\frac{1}{S_{ref}}\right)\sum\left(C_{Df}(FF)(IF)(S_{wet})\right) + C_{D\ misc} + C_{D\ L\&P}\right]\left(1 + \frac{CRUD}{100}\right) \quad (4\text{-}3)$$

Skin friction coefficients were first calculated and then corrected with *FF*s and *IF*s based on geometry layouts. XFOIL [14] was used to determine viscous upper and lower turbulent transition points in cruise conditions for each component. Component *IF*s were determined and applied to each component using Chapter 15.4.7 of Gudmundsson [3]. The *FF* of each component was determined using three different methods provided in Chapter 15.4 of Gudmundsson that were specific to each component. The miscellaneous drag component was then calculated and was comprised of contributions from the fuselage upsweep angle, nose gear, and main gear. Leakage and protuberance (L&P) drag contributions were analyzed last. A 10% margin, as recommended by Raymer [7], was added to account for leakage and protuberances because of the amateur-built nature of MULLET. Ultimately, because drag estimations of past ERAU DB aircraft were often found to be low, a "*CRUD*" factor of 60% was applied to account for uncertainties in the model. This *CRUD* factor was determined from Gudmundsson [3] in conjunction with historical ERAU DB *CRUD* factors needed to match flight test data.

4.4.1 Complete Parasitic Drag Build-Up

Once the parasitic drag of all the components was determined, the drag build-up yielded a total minimum drag coefficient of 0.0456 for Mission 2 cruise conditions; the breakdown is shown in Figure 4-3.

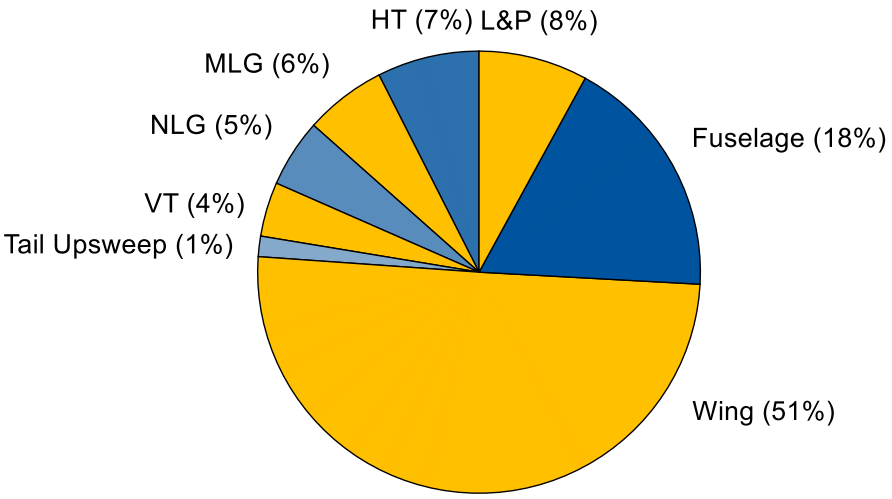

Figure 4-3: Mission 2 parasitic drag breakdown

The wing, with a 14% thickness-to-chord ratio, was the largest contributor to the aircraft's parasitic drag, as expected. Further efforts to reduce wing area and interference remained the focus of drag reduction. Improving aircraft manufacturing quality to minimize imperfections also remained a focus to reduce leakage and protuberance drag.

4.4.2 Lift to Drag

Lift and drag coefficients were calculated for each mission using an aircraft drag polar generated from XFOIL [14] and drag calculation data. This approach was further corrected for the quadratic increase in drag from high C_L conditions using Chapter 15.2.3 of Gudmundsson [3]. *L/D* ratios for each mission were then plotted against airspeed, as shown in Figure 4-4. All curves are in reference to cruise conditions at 1,400 ft MSL density altitude, the cruise altitude for the competition field in Wichita, Kansas in hot April

conditions. Based on the selected cruise airspeed, it can be seen for all missions that aerodynamic efficiency was traded for a high cruise airspeed. The highest cruise *L/D* was achieved in Mission 2, while the lowest was in Mission 3.

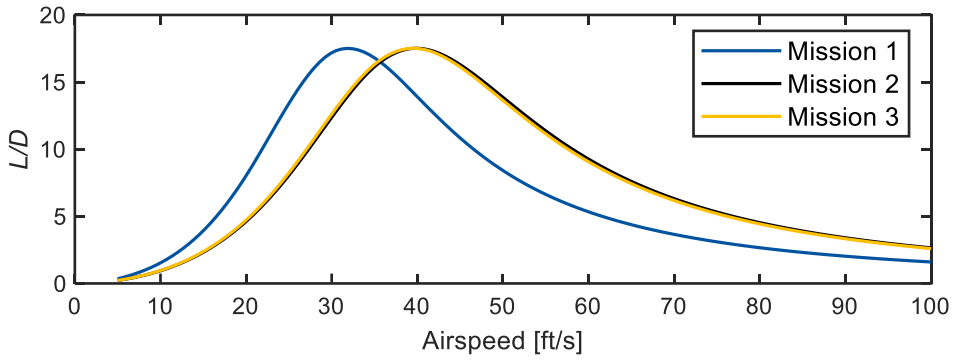

Figure 4-4: L/D ratio versus airspeed

4.5 Performance

The performance of the aircraft was limited by Requirements AC-05, AC-12, AC-18, M2-02, and M3-06. In addition, hardware selections for the propulsion system and avionics were limited by Requirements AC-08 to AC-13.

4.5.1 Propulsion System Selection

Though takeoff distance was the most critical requirement in the propulsion system sizing, it was decided that an increase in wing area could help meet this particular requirement. Therefore, sizing of the propulsion system was focused on the ability to deliver as many vials as possible within the given time for Mission 3. Because of the energy limit imposed by Requirement AC-12, a single motor was used.

To set a realistic goal for the number of vial packages that could be delivered in 10 minutes during Mission 3, the team used historical data to arrive at a total lap time of 75 seconds, takeoff to takeoff. This approach allotted the aircraft 60 flight seconds and 15 ground seconds to deliver each of the eight vial packages. Then, to size the motor, the 100 Wh propulsion power limit per Requirement AC-12 was divided by the 8-minute flight time. Assuming an 85% battery discharge by the end of the mission, the optimal average in-air power draw was calculated to be 637.5 W. Finally, an iterative airspeed and endurance model, accounting for the decrease in weight by 0.5 lb per lap as vial packages were delivered, was developed to analyze various motors using data from eCalc [4]. This analysis is shown in Table 4-11. Table 4-12 outlines the final propulsion system selections.

Table 4-11: Mission 3 motor performance accounting for payload deployment (15x10E propeller) [4]

Motor	M6 CODE12 400Kv	Hacker A50-16S^2 378kV	Hacker A50-14L Turnado 400kV	KDE 3520XF
Average Endurance [min]	7.75	8.20	7.80	7.66
Max Thrust [lb]	10.9	10.4	11.1	10.3
Est. Level Speed [ft/s]	91.0	88.0	92.4	85.1
Weight [lb]	0.551	0.716	1.00	0.540

Table 4-12: Propulsion system hardware selections

Component	Selection	Reasoning
Motor	Mad Components M6 Code 12 400Kv	Low weight, very close to meeting the required airspeed and endurance for Requirement M3-06
ESC	Avian 80 Amp SMART	High amperage capability, reverse thrust option to reduce landing roll to assist in Requirement M3-05
Battery	2x 4-Cell LiPo 3300 mAh (series)	This battery configuration was found to be optimal to meet Requirement AC-12 during thrust tests with selected motor
Propeller	15x10E, 16x10E, and 16x12E	Historically used propellers, adequate performance achieved in testing, further testing required for final selection

4.5.2 Takeoff, Climb, and Glide

Takeoff performance estimates were carried out for each mission. These estimates used the aircraft drag calculations with expected powerplant performance. Takeoff performance was analyzed using Chapter 17 of Gudmundsson [3] to iteratively calculate the takeoff distance. This process accounted for rolling resistance and drag in the takeoff configuration during the takeoff run. In addition, thrust changes during the takeoff run were accounted for using a cubic spline approximation. Figure 4-5 shows the takeoff distances for each mission. Additionally, these results show that with an initial conservative static thrust estimate of 10 lb, the design met the takeoff requirements with flaps deflected.

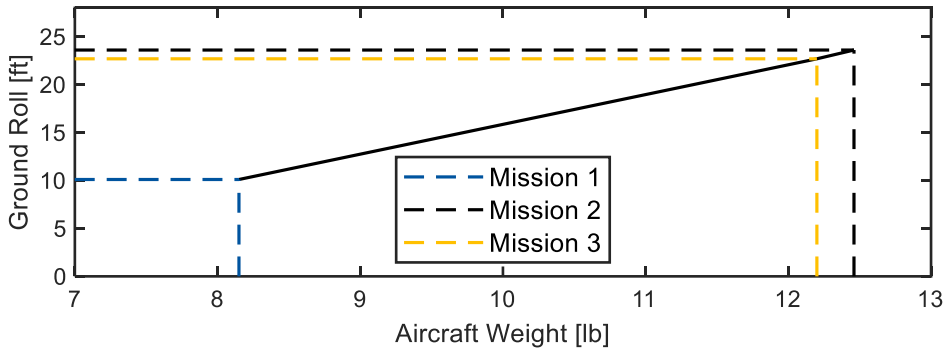

Figure 4-5: Ground roll versus takeoff weight

Climb analysis was completed using Raymer's methods [7] to calculate the ROC and AOC. Based on the flight pattern shown in Figure 3-1, it was desired for MULLET to climb to 100 ft AGL over a horizontal distance of 500 ft. In its heaviest configuration at the best achievable AOC, MULLET would fly at 36.6 ft/s

and climb at 1,096 fpm (18.3 ft/s). Using these values, MULLET could climb a total of 250 ft over a 500 ft forward distance, thereby satisfying the required ROC. For emergency performance, the drag addition of a windmilling propeller was accounted for using Gudmundsson's methods [3]. The previously created *L/D* plots were then adjusted for the increased drag from this windmilling propeller. The maximum glide distance of MULLET for a given altitude above ground level when operating at the mission altitude of 1,400 ft MSL is shown in Figure 4-6.

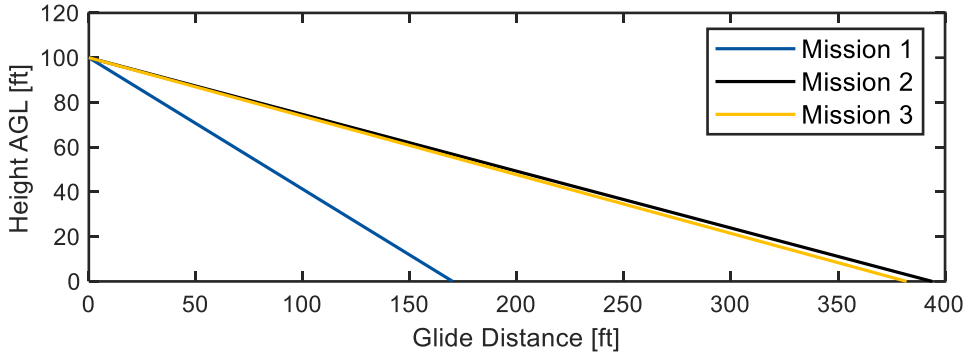

Figure 4-6: Maximum glide profile with windmilling propeller for all missions

4.6 Stability and Control

The stability and control MULLET was first analyzed using methods from Datcom [12] with some adaptations from Greiner [13]. Next, a model was created in Digital Datcom [15] to validate the initial calculations. Lastly, another model was created in Surfaces [16] for a more detailed analysis using a vortex lattice method. The stability axis sign convention, specified by Greiner, was used in all cases. Each of the stability derivatives were determined to be acceptable within the bounds discussed by Greiner. In addition, flight test analysis and pilot feedback confirmed that MULLET was stable enough to meet competition requirements.

4.6.1 Static Stability

Table 4-13 compares the primary stability derivatives from Datcom/Greiner, Digital Datcom, and Surfaces.

Table 4-13: Static stability values

Parameter	Variable	Datcom/ Greiner	Digital Datcom	Surfaces
Basic Lift Coefficient	C_{Lo}	0.1353	0.1650	0.1262
Lift Curve Slope [/deg]	$C_{L\alpha}$	0.08427	0.08756	0.08020
Basic Pitching Moment	C_{Mo}	-1.34×10^{-4}	-	-
Pitching Moment Slope [/deg]	$C_{M\alpha}$	-0.009936	-	-0.008310
Static Margin	$SM = -C_{M\_CL}$	0.1179	-	0.1036
Neutral Point (Power Off) [% MAC]	N_o	0.42	-	0.41
Side Force Derivative [/deg]	C_{Yb}	-0.006338	-0.007232	-0.009940
Directional Stability [/deg]	C_{Nb}	0.001923	0.002338	0.003020
Lateral Stability [/deg]	C_{lb}	-0.001553	-0.001174	-0.001050

For the fuselage to cruise at a 0-degree angle of attack to reduce drag, the required incidence angle of the wing was determined to be -1.5 degrees. To trim the aircraft for the Mission 2 cruise condition, the incidence angle of the horizontal tail was determined to be -0.5 degrees.

4.6.2 Stability CG Range

To evaluate the allowable CG range for sufficient aircraft stability, experimental data from a wing wind-tunnel test was used to correct the aircraft's neutral point of 42% MAC (Table 4-13) to 50% MAC (using the experimental lift coefficient, lift curve slope, moment curve slope, and zero-lift angle of attack explained in Section 8.1.2). Then, the neutral point was reduced by 10% to correct for power effects and by another 5% for a safety margin following Greiner [13]. Therefore, the aircraft's aft CG limit was 35% MAC. Then, Equation 4-4 was used to calculate the most-forward CG limit (with flaps).

$$\left(\tilde{x}_{CG\,fwd\,OGE}\right)_{\text{dirty}} = \widetilde{N_{o}}_{WP} + \left(C_{M_{C_{L\max}}}\right)_{\text{dirty}} = \widetilde{N_{o}}_{WP} + \frac{-\left(C'_{M_o} + C_{M_{\delta_e}}\delta_{e\text{-max up}} + \Delta C_{M\text{-wf}}\right)}{C_{L\text{-max dirty}}} \tag{4-4}$$

The forward CG limit was 17% MAC, which resulted in a stability CG range of 17% to 35% MAC.

4.6.3 Dynamic Stability

Longitudinal dynamic stability is characterized by the short period and long period (phugoid) modes. Lateral-directional dynamic stability is characterized by the spiral, Dutch roll, and roll convergence modes. These modes were analyzed using Surfaces [16], with the results shown in Table 4-14. The dynamic stability behavior was referenced to 14 CFR § 23.181 [2] and was found to be acceptable for all modes.

Table 4-14: Mission 2 (heaviest weight) dynamic stability analysis [16]

Mode	Time [s]	Time [s]	Criteria
Short Period	0.0676 to half	0.2247 to tenth	Acceptable per 14 CFR § 23.181(a)
Long Period (Figure 4-7)	95.71 to half	317.9 to tenth	Ample time for pilot control reaction, acceptable per 14 CFR § 23.181(d)
Spiral	31.09 to double	103.3 to 10x	Ample time for pilot control reaction, acceptable per 14 CFR § 23.181
Dutch Roll	0.1814 to half (0.3468 cycles)	0.6026 to tenth (1.1520 cycles)	Acceptable per 14 CFR § 23.181(b)
Roll Convergence	0.0128 to half	0.0426 to tenth	Acceptable per 14 CFR § 23.181

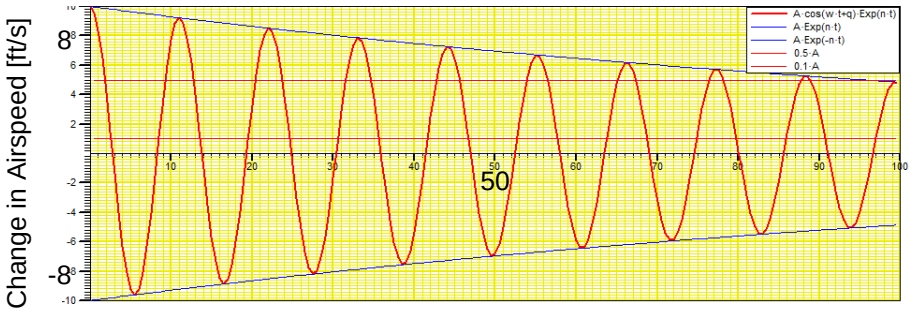

Time Since Disturbance [s]

Figure 4-7: Mission 2 long period mode [16]

4.6.4 Controllability

As discussed in Section 4.3, all control surface chord ratios were initially defined to be 30%. The deflection limits were determined to be 30 degrees based on the historical maximum attainable angle found during manufacturing. Surfaces [16] validated that a 30-degree deflection was acceptable for each surface. Although the flaps could be mechanically deflected to 30 degrees, they were only deflected to 15 degrees under normal operation for takeoff and landing.

Table 4-15 compares the primary control derivatives between hand and Surfaces approximations. Each of the derivatives were determined to be acceptable according to Greiner [13]. In addition, flight test analysis and pilot feedback confirmed that MULLET was controllable to meet competition requirements.

Table 4-15: Controllability analysis (all units /deg)

Parameter	Variable	Hand	Surfaces
Aileron Rolling Power	$C_{l\_\delta a}$	-0.001341	-0.006050
Lift Variation with Elevator	$C_{L\_\delta e}$	0.009148	0.01000
Elevator Pitching Power	$C_{M\_\delta e}$	-0.01568	-0.02380
Side Force Variation with Rudder	$C_{Y\_\delta r}$	0.002826	0.004800
Rudder Yawing Power	$C_{N\_\delta r}$	-0.001313	-0.002390
Lift Variation with Flap	$C_{L\_\delta f}$	-	0.04020
Flap Pitching Power	$C_{M\_\delta f}$	-	0.0009920

Finally, the calculated control power of each surface was analyzed. The elevator analysis is shown in Table 4-16. The rudder could sustain a sideslip of 20.5 degrees and required only 8.5 degrees of deflection to overcome adverse yaw. In addition, the ailerons could produce a minimum roll rate of 16.76 degrees per second (at stall) and a maximum roll rate of 25.07 degrees per second (at Mission 2 cruise). Each of the previous analyses determined that the control surfaces were adequately sized to meet competition requirements.

Table 4-16: Elevator required at maximum weight (12.46 lb) with most forward CG (17% MAC) [16]

Flight Condition	V_{inf} [ft/s]	α [deg]	Trim δ_e [deg]
Takeoff & Landing (15 deg flaps)	33.4	10.63	-15.6
Rejected Landing (15 deg flaps)	39.4	4.76	-10.2
Cruise	92.4	0.92	-3.1

4.7 Internal Layout

The internal layout of the propulsion system, batteries, and avionics was chosen to maximize the usable payload and subsystem volume, while also maintaining manufacturability and ease of access to each component for troubleshooting.

4.7.1 Vaccine Syringe Staging Mechanism

To maximize the Mission 2 score, it was important that the fabric bags took advantage of all available payload volume. For this reason, the fabric bags were sized based on the outer dimensions of the fuselage, with the goal of the bags forming around bulkheads and the VVPDM when loaded with the syringes.

4.7.2 Vaccine Vial Package Delivery Mechanism

With the one-level conveyor belt and door slide having been selected as the best concept for the VVPDM, the subsystem was then designed to fit inside the proposed payload bay volume of 5 in by 5 in by 36 in. The system utilized a timing belt with two parallel guide rails to store and transport the vial packages to an actuating door that deployed them safely to the ground, per Requirement M3-07. Two potential methods were considered to drive the conveyor belt, as outlined in Table 4-17.

Table 4-17: VVPDM conveyor belt drive method selection matrix

Option	Pros	Cons
98 rpm Econ Gear Motor	Very fast, does not require gear reduction	Heavy, bulky, and requires an ESC (more power and more weight)
360-deg Servo	Easily programmable using Arduino, less power intensive, lightweight	Slower, separate mount/shaft must be designed and manufactured

The 360-degree servo was selected to conserve weight and volume. First, a prototype VVPDM was constructed to evaluate the concept, as shown in Figure 4-8.

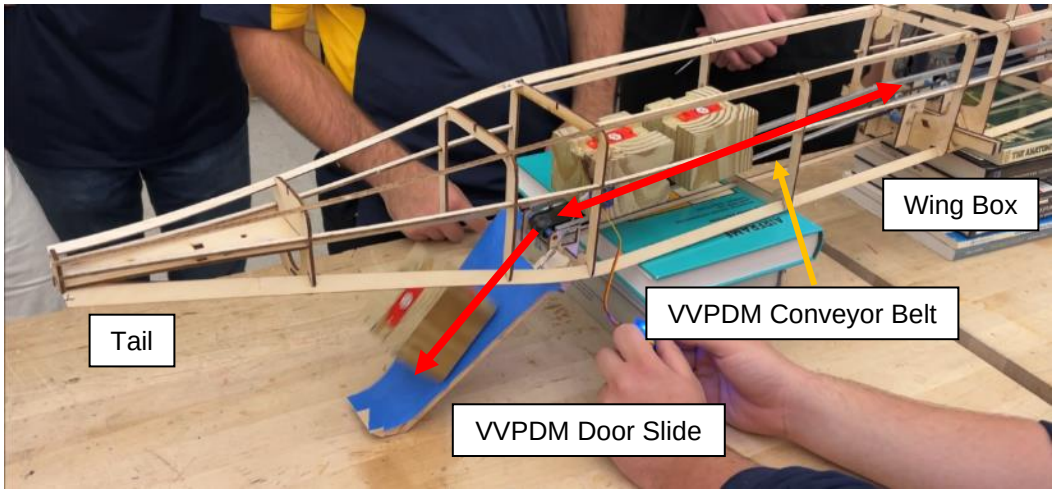

Figure 4-8: VVPDM prototype

The prototype helped to identify the strengths and weaknesses of the design and provided a good foundation to begin a CAD model. The prototype allowed for further refinement of the components to be used, as shown in Table 4-18. 3M VHB tape with a width of 1 in was selected to adhere to the vial packages to the belt because it was strong enough to keep the vials attached in flight but still allowed the vial packages to detach and roll onto the door slide. Another set of wooden guide rails was used on the two upper corners of the vials to further restrain them during flight. These upper guides were collapsible to conserve syringe

payload volume for Mission 2. An Arduino Nano (a commonly used microprocessor) was used to operate the VVPDM by controlling the belt rotation and actuating the door. The upper surface of the rear door acts as a slide contoured to allow the vial package to safely roll to the ground.

Table 4-18: VVPDM component selections

Component	Selection	Reasoning
Conveyor Belt	2 mm GT2 timing belt, 6 mm width	High strength, lightweight, standard size
Guide Rails	6061-T6 Al L-rail, 0.25 in width	Strong, low friction with vials, commercially available
360-deg Servo	Parallax feedback 360 high-speed servo	Fast, adequate torque to deploy the vials, internal encoder
Door Servo	Corona DS939HV metal gear	Light, adequate torque to actuate the door
VVPDM Controller	Arduino Nano with Spektrum receiver	Small compact form, has enough inputs and outputs for the task
Spools	20 tooth, 2 mm GT2 idler pulley, 6 mm width	Lightweight, commercially available, integrates with 2 mm GT2 timing belt
Shaft Hardware	#10-32 thread: • 18-8 stainless steel half-threaded shaft, 2.5 in length • 3/8 in x 15/64 in nylock • 5/16 in x 7/64 in hex nut	Lightweight, common thread (spare parts and tools easily accessible)
Belt Adherence	3M VHB Tape, 1 in width	Strong adhesive, worked well to transport and deploy vials during prototype testing

4.7.3 Avionics

The remaining internal layout of the aircraft was comprised of the propulsion system hardware and avionics. The batteries were placed directly in front of the wing box for proper CG, below the VVPDM conveyor belt to take advantage of otherwise unusable payload volume. The ESC was placed in the unusable payload volume of the nose, directly behind the firewall; this location also allowed for an air duct from the motor cowl to provide in-flight cooling. In addition, the Spektrum receivers that controlled the aircraft and sent signals to the Arduino Nano to operate the VVPDM were placed in the left and right wings, respectively, to take advantage of available volume outside the fuselage. The internal layout is shown in Figure 4-9.

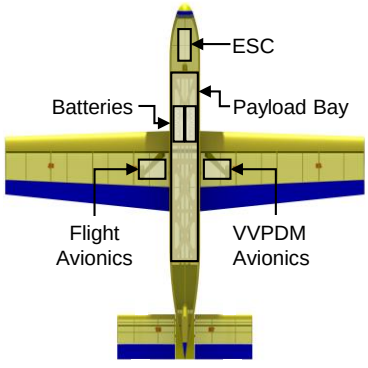

Figure 4-9: Fuselage internal layout

4.8 Risk Analysis of Uncertainties

Systems and features of the aircraft that influence the overall reliability, safety, and performance in competition were analyzed for risk, seen in Table 4-19. These items were assessed based on their likelihood to occur and the severity of the failure, where five was a total loss, four was significant damage, three was a totally failed mission, two was a partially failed mission, and one was an inconvenience. The product of the likelihood and severity yielded an overall risk factor. Risk management strategies, including structural testing, propulsion testing, quality control, and thorough preflight checks, proved to be adequate for early iterations of MULLET. Additionally, the iterative testing approach revealed failure points that were not originally considered in the design, which will yield a better performance in competition.

Table 4-19: Risk analysis

Risk	Likelihood x Severity = Risk Factor	Mitigate, Minimize, or Accept
Wing Box Structural Failure	3 x 5 = 15	Minimize by further structural analysis
Fuselage Structural Failure	2 x 5 = 10	Minimize by further structural testing
CG Shift from VVPDM Conveyor Failure	2 x 5 = 10	Minimize by further VVPDM testing
Overlooked Manufacturing Defects	2 x 4 = 8	Minimize by quality control and inspect
VVPDM Failure to Deploy Vial Packages	2 x 3 = 6	Minimize by further VVPDM testing
Propulsion Shortfall of 25 ft Takeoff	2 x 3 = 6	Minimize by further propulsion testing
Control Surface Servo Failure	1 x 4 = 4	Mitigate by purchasing reputable servos
Crosswind Takeoff/Landing Condition	4 x 1 = 4	Accept due to Wichita, Kansas weather
CG Shirt from VSSM Constraint Failure	1 x 4 = 4	Minimize by further VSSM testing
Battery Capacity Loss In-Flight	1 x 2 = 2	Mitigate with on-board telemetry

4.9 Predicted Mission Performance

Table 4-20 summarizes the projected team scores.

Table 4-20: Preliminary design predicted team score

Mission	Team Performance	Est. Fly-Off Maximum	Predicted Team Score
M1	Pass	N/A	1.00 (Equation 3-1)
M2	70 syringes per minute	98 syringes per minute	1.71 (Equation 3-2)
M3	8 successful deployments	10 successful deployments	2.80 (Equation 3-3)
GM	30 seconds	15 seconds	0.50 (Equation 3-4)
Total	**N/A**	**N/A**	**6.01**

5 Detail Design

After the conceptual design, preliminary design, and initial flight test analysis were complete, the external geometry of the aircraft was finalized under the terms of the DBF competition rules and team requirements.

5.1 Final Aircraft Dimensions

The final aircraft configuration is shown in Figure 5-1 and the overall dimensions are shown in Table 5-1.

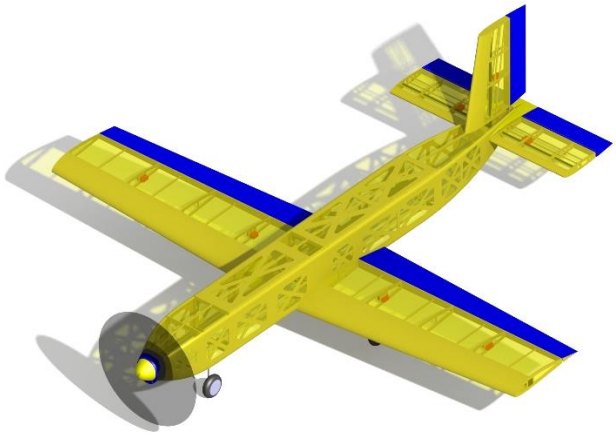

Figure 5-1: Final design of MULLET

Table 5-1: Final aircraft dimensions

Parameters	Fuselage	Parameters	Wing	HT	VT
Length [in]	71.50	**Airfoil**	SD7062	NACA-0012	NACA-0012
Width [in]	6.00	**Span [ft]**	5.93	2.23	1.16
Height [in]	6.00	**Root Chord [in]**	16.42	8.91	11.39
Nose Length [in]	12.82	**Tip Chord [in]**	11.49	8.91	8.54
Payload Bay [in]	36.00	**Area [ft^2]**	6.90	1.65	1.10
Tail Length [in]	22.68	**Aspect Ratio**	5.1	3.0	1.4
		MAC [in]	14.10	8.91	10.03
		FS LE MAC [in]	26.46	62.38	61.24
		BL MAC [in]	16.75	7.22	0
		FS AC [in]	30.58	64.55	63.75

5.2 Structural Characteristics

To meet the structural requirements, a semi-monocoque structure consisting of wood stringers, longerons, formers, ribs, spars, and skin was utilized. Commercially available carbon fiber tubes were used for the spars and landing gear to transfer the major loads to the load paths shown in Figure 5-2. The team attempted to balance the weight, strength, and manufacturability of the structure to provide the optimal configuration that could accomplish all mission requirements and goals. The subsections below detail the structural analysis and integration of the major aircraft components.

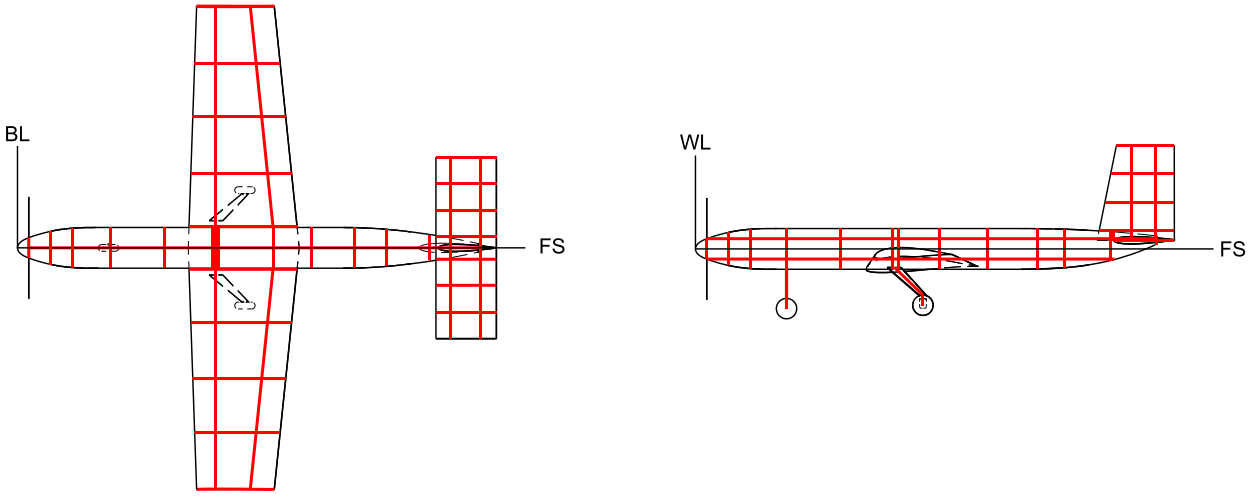

Figure 5-2: Aircraft load paths

5.2.1 Fuselage

The fuselage structure utilized a semi-monocoque design for simplicity while also allowing for flexibility to carry payload. Plywood formers made up the cross-section, with balsawood stringers and plywood ventral longerons connecting these formers. Balsawood shear panels were installed on the sides and bottom of the fuselage to carry the shear and torsion loads. 3D-printed and hotwire-cut foam structures were used for non-structural geometry. In the fuselage, the most critical component was the wing box and, specifically, the wing carry-through. This structure accepted both wings and was the main point of load transfer between the wings and fuselage.

A linear FEA was performed on the wing carry-through using FEMAP Nastran [17] to validate the stresses in the structure, shown in Figure 5-3. The model was meshed using TET10 elements and was loaded by idealizing the wing loading and finding the reactions at the wing box. A 5 g load factor was applied in the heaviest configuration to ensure a safety factor of 1.5 to the highest load measured in historical ERAU DB flight testing of 3.4 g and a safety factor of 2 to the 2.5 g load per Requirement AC-02. Because the wing carry-through self-reacts the bending moment, the model was constrained by fixing the upper flange corners in space.

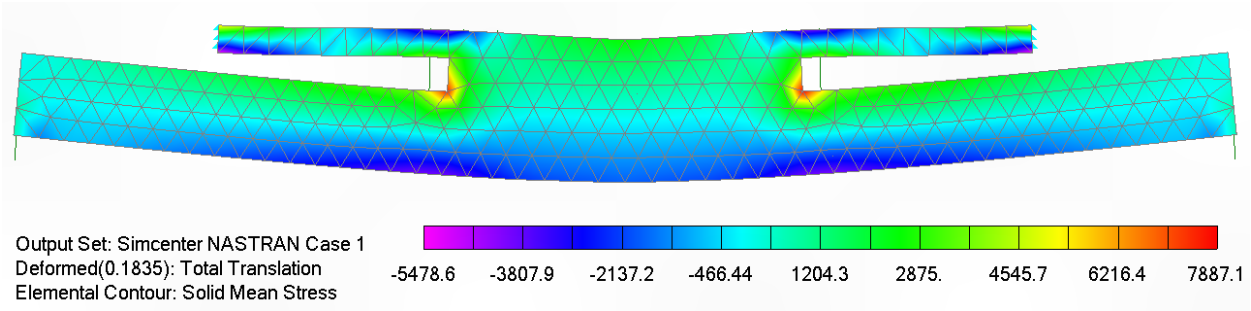

Figure 5-3: Wing carry-through stress FEA (deflections not to scale, stresses with opposite sign) [17]

The maximum tensile stress was found to be 98% of the listed ultimate tensile strength of 1/8 in 3-ply birch wood (7,900 psi versus 8,020 psi) [18]. The maximum compressive stress was found to be 94% of the listed ultimate compressive strength (5,500 psi versus 5,800 psi). Although high, the maximum stresses were near those expected for a high safety factor applied to the load. The wing carry-through design was deemed acceptable to move forward with the testing plan explained in Section 7.2.3.

5.2.2 Wing

A linear FEA was performed using FEMAP Nastran [17] to validate the stresses in the main wing spar, shown in Figure 5-4. The model was loaded with a lift distribution estimated using Schrenk's method with a 5 g load factor applied in the heaviest configuration to match the previous wing carry-through analysis.

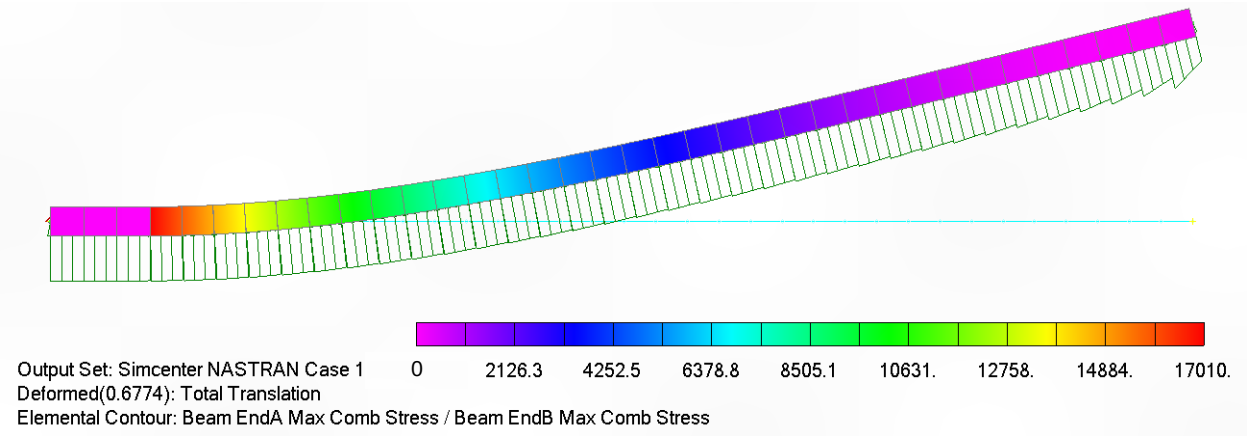

Figure 5-4: Wing spar stress FEA (deflections not to scale) [17]

The maximum combined beam stress was found to be approximately 17,000 psi; this value was 20% of the manufacturer's listed ultimate tensile and compressive strength of 86,000 psi [19]. The wingtip deflection of 0.68 in per side was expected at this loading based on historical ERAU DB wingtip deflections using the same carbon fiber tube.

5.2.3 Landing Gear

The carbon fiber landing gear had to support the full aircraft weight on the ground, resist impact landing loads, and maintain directional stability while taxiing. The landing gear structure was integrated into the wing spars to provide simpler load paths in the airframe.

A linear FEA was performed on the main landing gear using FEMAP Nastran [17] to validate the stresses in the structure, shown in Figure 5-5. The model was meshed using TET10 elements and was loaded with a vertical bearing force applied to the axle location. The top of the model was constrained to its interface on the main wing spar. A 2 g load factor was applied in the heaviest configuration.

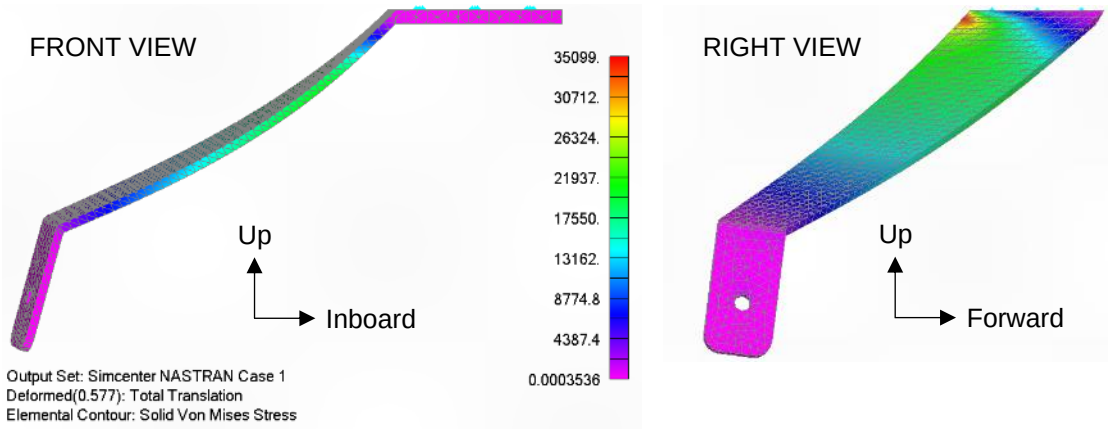

Figure 5-5: Right main landing gear stress FEA (deflections not to scale) [17]

The maximum Von Mises stress was found to be approximately 35,000 psi; this value was 5% of the listed ultimate strength of 12k carbon fiber tow at 711,000 psi [20]. The corresponding deflection was found to be approximately 0.58 in. These values were acceptable to accomplish the mission criteria. It should be noted that this analysis did not account for the matrix composition and assumed that the landing gear was fabricated of solid cardon fiber tow; therefore, the actual stress and deflection were expected to be larger than that predicted by the FEA. This assumption was made due to inadequate time and money for the team to measure the actual material properties. Still, the FEA results give a reasonable estimation of the landing gear's performance. The actual gear will be tested according to Section 7.2.3.

5.2.4 Empennage

The tail structure in MULLET was like that of the wing design. All tail surfaces were balsa built-up with removable main spars. The fuselage tail box structure received the spars, wiring, and alignment tabs. Mounting screws then secured the alignment tabs of the horizontal tail and were bolted into the vertical tail to secure the surfaces to the fuselage and support the torsional loads. The tail box is shown in Figure 5-6.

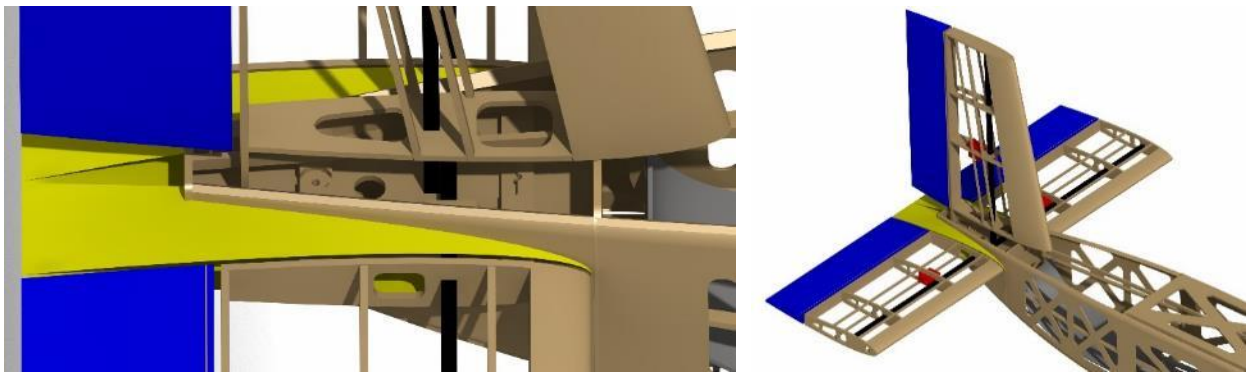

Figure 5-6: Tail box structure

5.3 Systems

The following sections outline the integration of each component into the full aircraft system.

5.3.1 Wing and Empennage

In accordance with Requirement AC-19, the main spar of the wing was permanently bonded to the wing, thereby allowing the entire wing assembly to be removed from the wing carry-through structure. The aft spar of the wing, located at the flap hinge line, contained an anti-rotation pin that connected to the nearest bulkhead aft of the wing box. This removable wing assembly is shown in Figure 5-7. The anti-rotation pin carried the torsional moment produced by the wing in addition to securing the wing from sliding off the wing carry-through during flight. The tail assembly, as described previously in Section 5.2.4, is also shown in Figure 5-7. All control surfaces were connected to the wings and tail using commercially available plastic hinges with a DS105CLHV servo to actuate each surface.

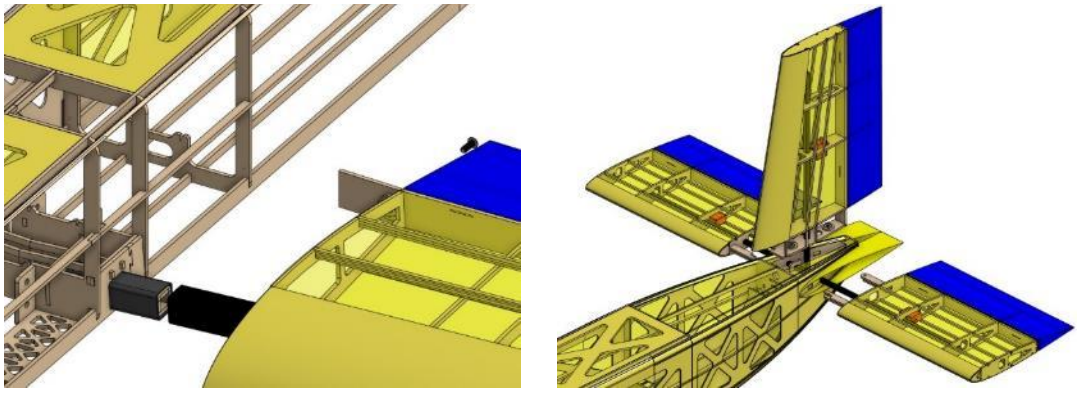

Figure 5-7: (Left) wing box and anti-rotation pin system integration, (right) empennage system integration

5.3.2 Propulsion System and Avionics

The propulsion system and avionics are integrated according to the wiring diagram shown in Figure 5-8.

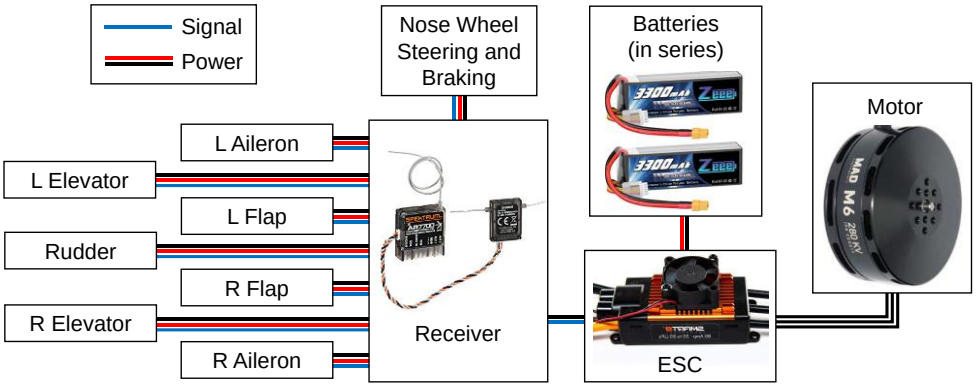

Figure 5-8: Propulsion system and avionics wiring diagram

5.3.3 Motor Cowl and Firewall

A 3D-printed cowl, shown in Figure 5-9, was incorporated into the aircraft design with a duct to provide sufficient cooling to the motor and ESC in all flight conditions. The ram air was redirected into the duct and distributed around the motor's base. Auxiliary holes in the firewall provided a constant flow of air across the ESC's heatsink to mitigate the risk of overheating.

Figure 5-9: (Left) motor cowl and (right) firewall

Few resources exist for brushless motor cooling, so the area of the duct was sized using Raymer's piston engine cooling approach [7]. Equation 5-1 was used to determine the required cooling area. Then, the exit area of the cooling system was taken to be 110% of the previously calculated inlet area. During the flight test, the temperature of the motor and ESC were measured to validate the selected inlet and outlet areas.

$$A_{cooling} = \frac{bhp}{2.2\ V_{climb}} \tag{5-1}$$

5.3.4 Vaccine Syringe Staging Mechanism

The VSSM needed to fit as many syringes in the payload bay as possible in the given payload volume. A single top door would interfere with the wing box bulkheads, significantly impacting the aircraft's strength. Consequently, two doors were used to maximize payload volume in front of and behind the wing box. The bags were then sized for the length of the front and rear doors measuring 14.50 in and 20.25 in, respectively. Additionally, the width was set to 6 in, the outer width of the fuselage, with the goal of the bags forming around the bulkheads and VVPDM when loaded with syringes. The height was intentionally left long, at 12 in, so when loaded the top could be rolled to secure the syringes inside the bags, with rubber bands placed around the bags to prevent the top from opening in flight. It was also determined that support from the bulkheads was sufficient to avoid any movement of the bags when fully loaded with syringes, ensuring a safe CG was maintained during flight. For storage during other missions the bags were rolled up and secured in the nose of MULLET.

Figure 5-10: VSSM installed in the aircraft

5.3.5 Vaccine Vial Package Delivery Mechanism

The VVPDM, consisting of the door slide and conveyer belt, was mounted to the aft fuselage bulkheads. To conserve payload volume, the lower half of the conveyer belt was routed below the wing box using idlers to guide its path. The 360-degree servo was mounted to the nose landing gear bulkhead with a 3D-printed mount that also functioned as the tensioning mechanism. By loosening the conveyor belt, the VSSM could store syringes between the guide rails of the VVPDM. The upper guide rails mounted to the bulkheads and secured the vial packages in flight by extending into place with a manual linkage. The door slide and most-aft conveyer belt idler were mounted to a single aluminum axle, allowing the vial packages to transition seamlessly from the conveyer belt to the slide. Finally, the lower surface of the door conformed to the outer mold line of the empennage to preserve the existing aerodynamics. Dimensions of the VVPDM are shown in Table 5-2. The VVPDM is shown integrated into the aircraft in Figure 5-11.

Table 5-2: VVPDM dimensions

Parameter	Value
Guide Rail Length [in]	38
Width Between Guide Rails [in]	2
Belt Length [in]	82.6
Door Length [in]	9
Subsystem CG FS [in]	23.9
Total Subsystem Weight [lb]	0.78

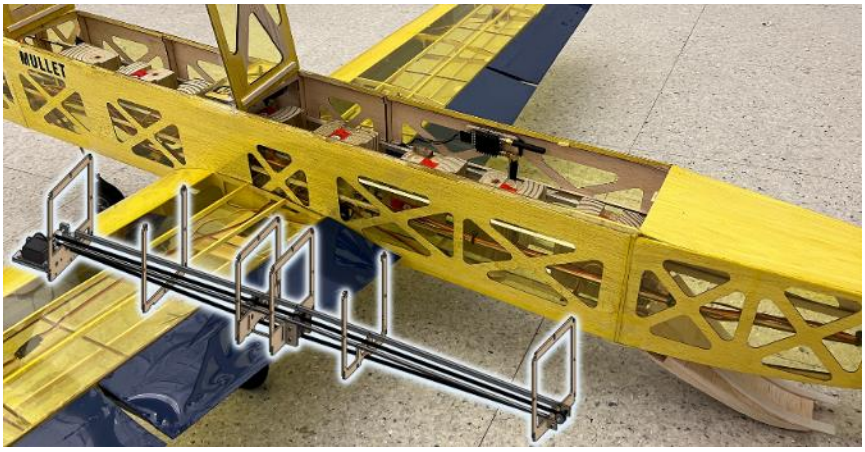

Figure 5-11: VVPDM system integration

5.4 Weight and Balance

To refine the preliminary weight estimate, historical mass property values were collected from the 2020 [5] and 2021 [6] ERAU DB competition aircraft. Both aircraft carried a modest payload (4.50 lb and 8.00 lb, respectively) and had a top airspeed comparable to MULLET. Because MULLET was sized between these two aircraft, their component weights were averaged to obtain an initial weight and balance. Table 5-3 compares these values and shows the CG location of each component on MULLET.

Table 5-3: Empty weight and balance compared to past ERAU DB average component weight [5] [6]

Component	W [lb] Past ERAU DB	W [lb] MULLET	FS [in] MULLET
Wing	1.03	1.03	30.22
Horizontal Tail	0.38	0.38	64.01
Vertical Tail	0.32	0.31	62.65
Fuselage	3.19	2.90	29.48
Landing Gear	0.69	0.81	23.39
Propulsion	1.08	0.55	1.56
Avionics	0.58	0.62	31.71
Empty Weight	**7.26**	**6.60**	**29.49 (38% MAC)**

As explained in Section 4.2, the propulsion system limited the empty weight of the aircraft to 6.60 lb. The actual weight of MULLET Iteration 1 was under this limit meaning that the propulsion system should perform to meet the mission requirements.

While it was initially desired to design the aircraft with a payload fraction close to the historical average (0.50 shown in Table 4-1) to increase the scores for Missions 2 and 3, the greatest payload fraction obtained in the iterative design methodology was 0.35. This outcome was largely because of the limits imposed by Requirements AC-05 and AC-12.

To maintain the desired CG of 30% MAC, the propulsion battery and payload must shift within the fuselage between each mission. These two components significantly impacted the balance of the aircraft because of their sizable weights and position relative to the desired CG. Table 5-4 summarizes the positions of the propulsion battery and payload for each mission.

Table 5-4: Mission weight and balance for CG at 30% MAC (FS 28.31 in)

Mission	Component	Weight [lb]	CG FS [in]
Empty	**Empty**	**6.60**	**29.49**
M1	Batteries	1.55	23.28
	Total	**8.15**	**28.31**
M2	Batteries	1.55	25.26
	Syringes	4.31	27.60
	Total	**12.46**	**28.31**
M3	Batteries	1.55	25.14
	Vial Packages	4.05	27.60
	Total	**12.20**	**28.31**

5.5 Final Design Performance

Table 5-5 summarizes the predicted flight performance of the final aircraft design for each flight mission.

Table 5-5: Final design predicted mission performance

Parameter	M1	M2	M3
Gross Weight [lb]	8.15	12.46	12.20
Ground Roll [ft]	6.31	23.61	20.69
Power Required [W]	1100	1300	1300
Thrust Required [lb]	11.2	11.2	11.2
Thrust to Weight	1.37	0.90	0.92
Wing Loading [lb/ft^2]	1.18	1.81	1.77
Rate of Climb [fpm]	1800	1200	1200
$C_{L\text{-}cruise}$	0.13	0.20	0.15
$C_{D\text{-}cruise}$	0.0618	0.0574	0.0576
L/D_{cruise}	2.03	3.40	3.33
Cruise Airspeed [ft/s]	110	110	92.4
Lap Time [s]	30	30	75

Lastly, Table 5-6 summarizes the predicted team scores. Despite the greatest possible fly-off score being 7.00, the predicted final team score of 6.01 is competitive with historical fly-off scores. The design of MULLET strikes a balance between each flight mission. Further flight tests will help to improve this score leading up to the fly-off, as explained subsequently in Section 7.

Table 5-6: Refined predicted team score

Mission	Team Performance	Est. Fly-Off Maximum	Predicted Team Score
M1	Pass	N/A	1.00 (Equation 3-1)
M2	70 syringes per minute	98 syringes per minute	1.71 (Equation 3-2)
M3	8 successful deployments	10 successful deployments	2.80 (Equation 3-3)
GM	30 seconds	15 seconds	0.50 (Equation 3-4)
Total	**N/A**	**N/A**	**6.01**

5.6 Drawing Package

The following section provides detailed drawings of MULLET and its subsystems, including the VSSM and VVPDM. All drawings were made with Onshape [21].

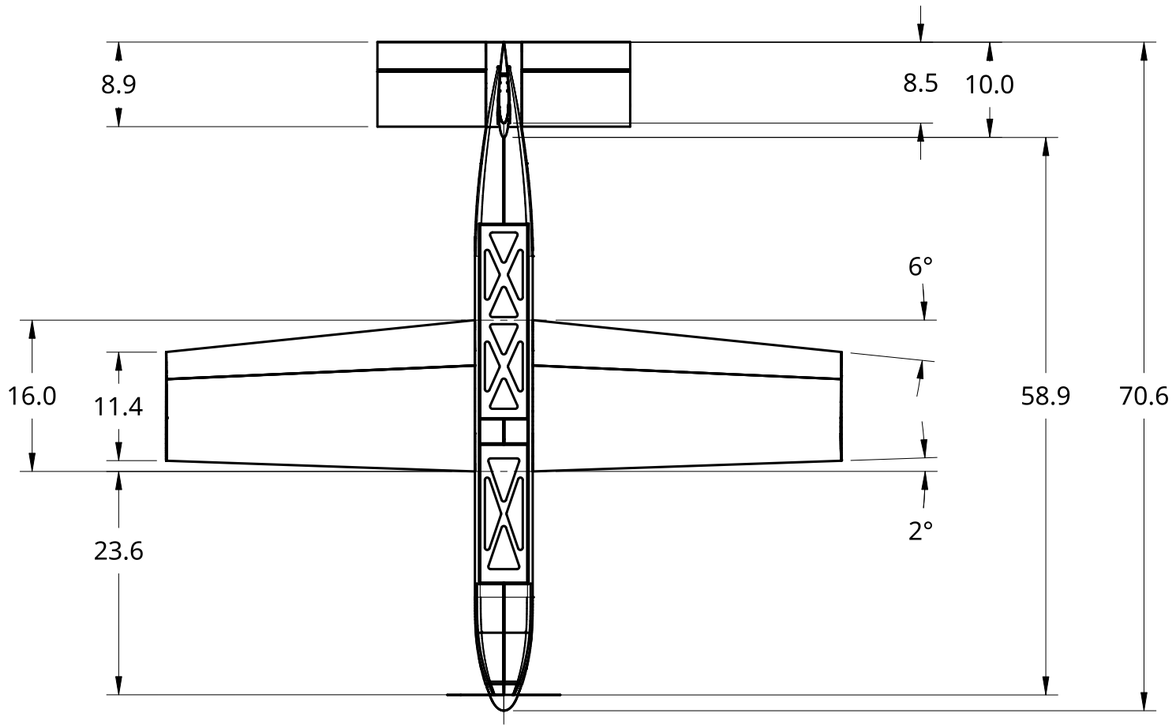

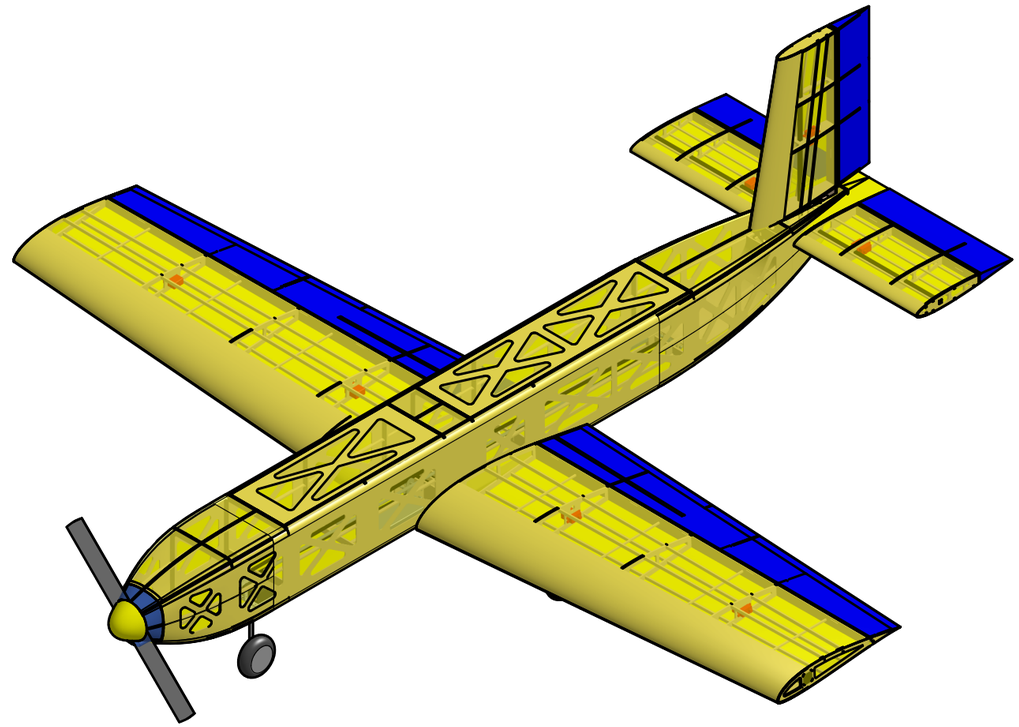

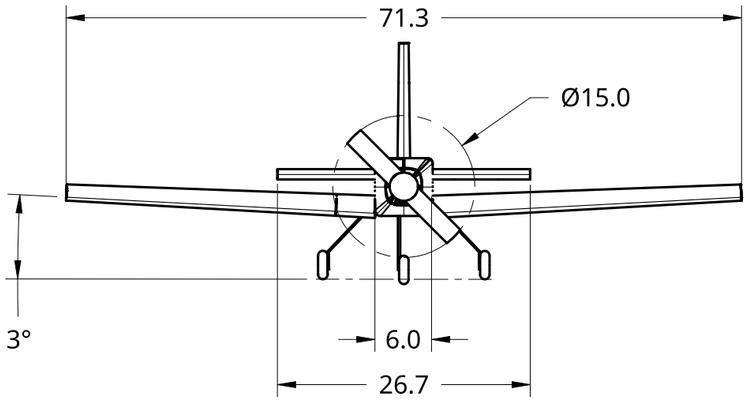

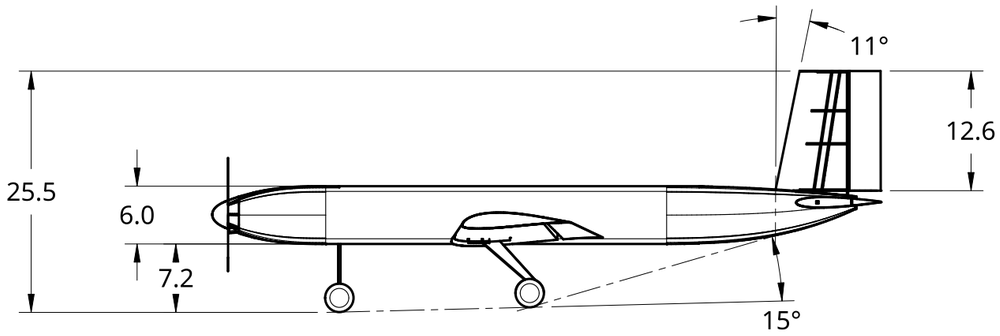

UNLESS OTHERWISE SPECIFIED, DIMENSIONS ARE IN INCHES .XX = ±.0- .XXX = ±.00- .XXXX = ±.000- ANGULAR = ± ° FRACTIONAL = ± SURFACE FINISH		NAME	DATE
	DRAWN	VICTOR CHANG	02/17/2022
	CHECKED	JOSEPH AYD	02/23/2022
	APPROVED	NOAH PECOR	02/23/2022
DO NOT SCALE DRAWING			
BREAK ALL SHARP EDGES AND REMOVE BURRS			
THIRD ANGLE PROJECTION	MATERIAL	FINISH	

EMBRY-RIDDLE DESIGN, BUILD, FLY

TITLE
EMBRY-RIDDLE AERONAUTICAL UNIVERSITY
DAYTONA BEACH
2021-22 AIAA DBF

SIZE	DWG NO.	REV.
B	AIRCRAFT 3-VIEW	1

SCALE	WEIGHT	SHEET
1:16		1 of 4

SYSTEM LIST

#	QTY.	NAME	DESCRIPTION
1	1	NOSE CONE	
2	1	PROPELLER	NYLON
3	1	MOTOR	MAD COMPONENTS M6C12 IPE 400KV
4	1	RIGHT WING	BALSA, BASS, CARBON FIBER
5	1	LEFT WING	BALSA, BASS, CABRON FIBER
6	1	LEFT HORIZONTAL STABILIZER	BALSA, BASS
7	1	RIGHT HORIZONTAL STABILIZER	BALSA, BASS
8	1	HORIZONTAL STABILIZER SPAR	CARBON FIBER
9	1	VERTICAL STABILIZER	BALSA, BASS
10	1	PAYLOAD DOOR	BALSA, TEFLON
11	2	BATTERY	ZEEE 4S 3300 mAh LiPo BATTERY
12	1	PAYLOAD CONVEYOR	BASS, ALUMINIUM, NEOPRENE
13	1	FUELAGE	BALSA, BASS, PLYWOOD
14	2	CANOPY	BALSA
15	1	NOSE LANDING GEAR	STEEL, FOAM, E/Z BRAKE SYSTEM

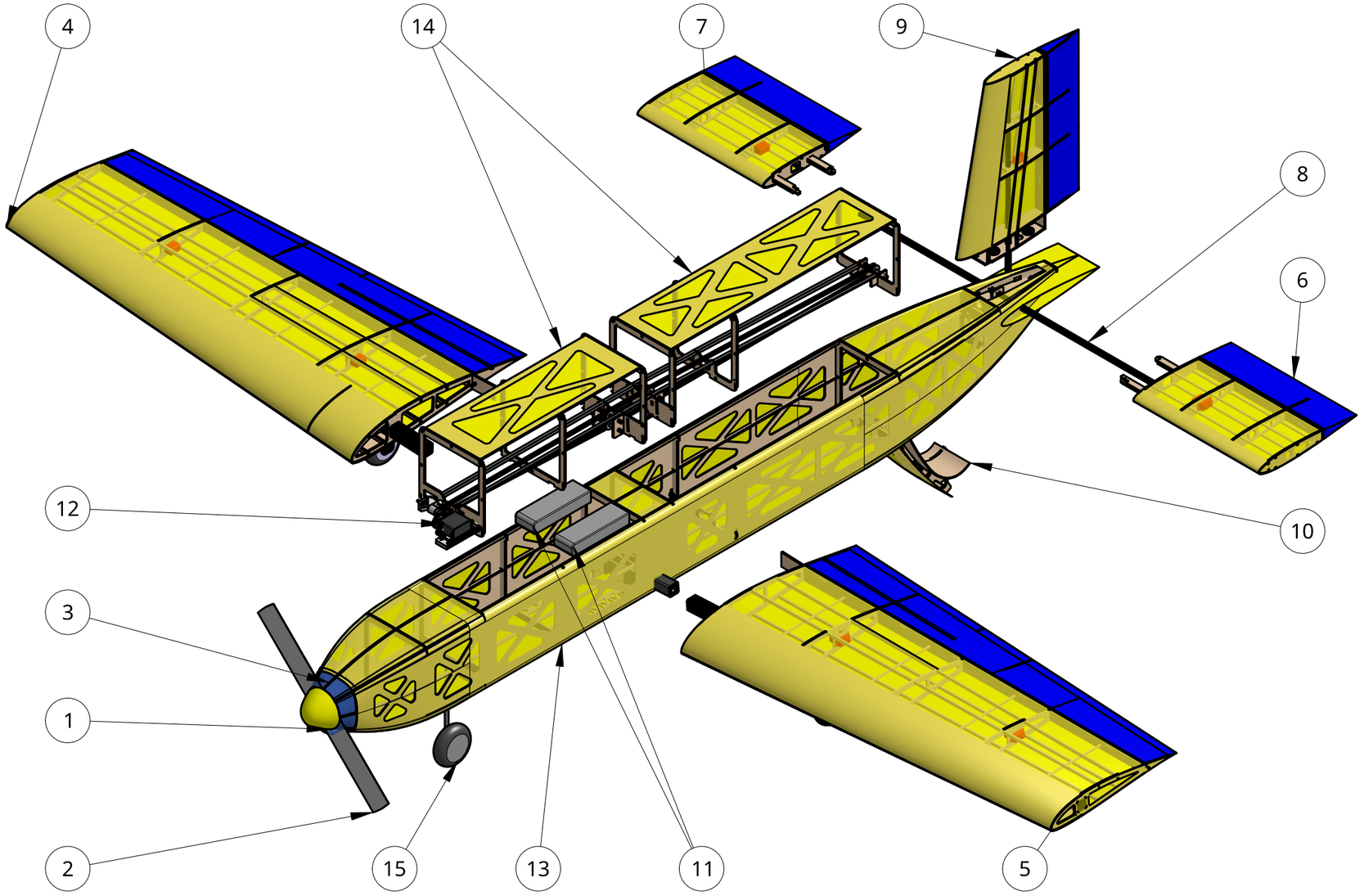

DWG NO.	SIZE	SCALE	SHEET	REV.
AIRCRAFT SUBSYSTEM	B	1:8	2 of 4	1

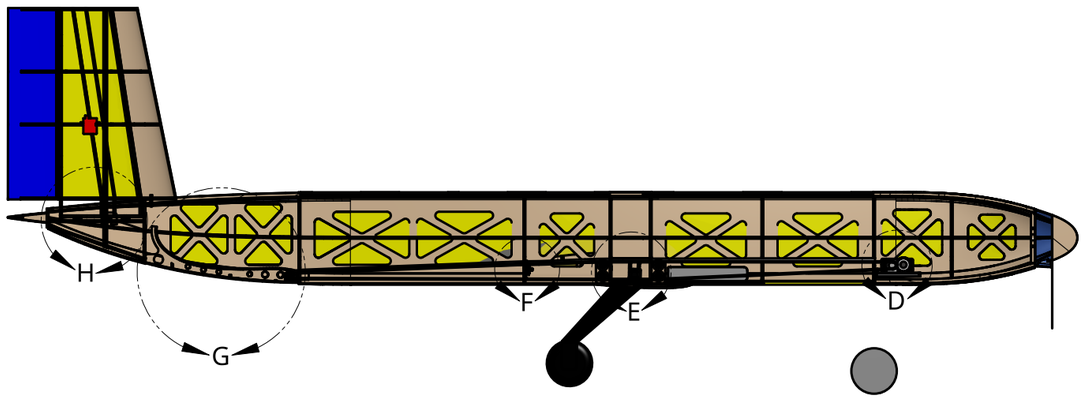

SECTION C - C

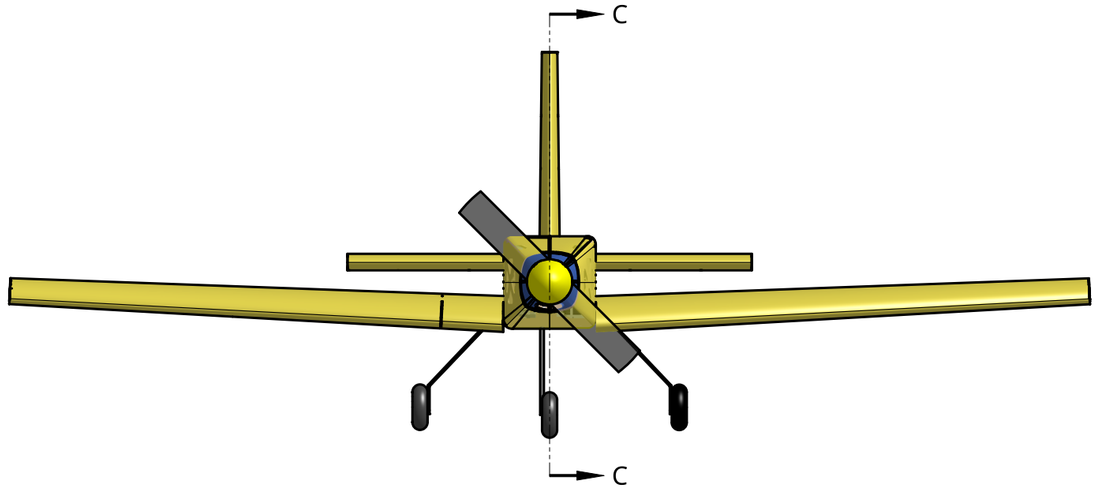

TAIL BOX

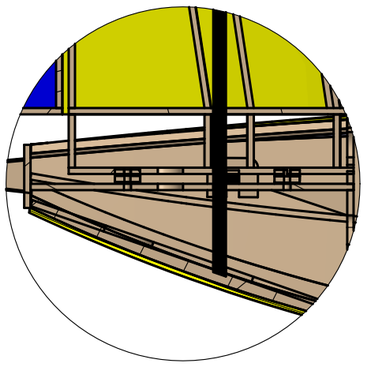

DETAIL H
SCALE 1:3

PAYLOAD DOOR

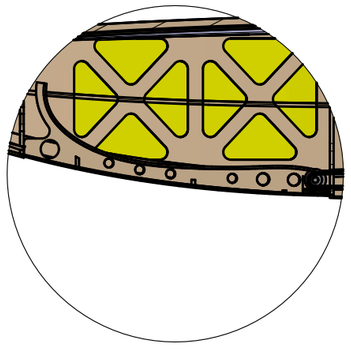

DETAIL G
SCALE 1:5

WING ANTI-ROTATION PIN

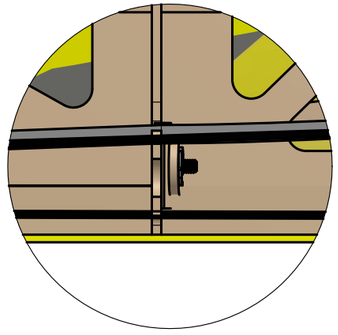

DETAIL F
SCALE 1:2

WING BOX AND SUBSYSTEM IDLERS

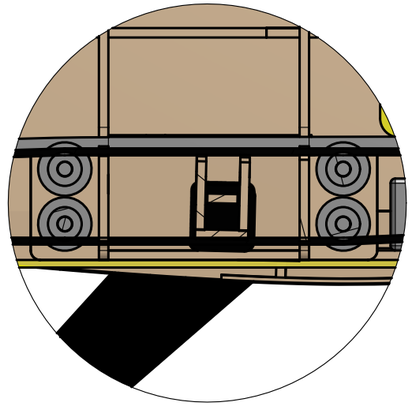

DETAIL E
SCALE 1:2

SUBSYSTEM SERVO ASSEMBLY

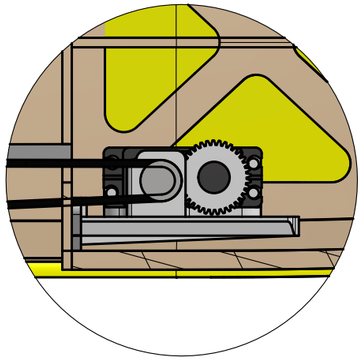

DETAIL D
SCALE 1:2

DWG NO.	SIZE	SCALE	SHEET	REV.
AIRCRAFT DETAIL	B	1:10	3 of 4	1

BILL OF MATERIALS		
#	QTY.	PARTS
1	1	2 MM GT2 TIMING BELT, 6 MM WIDTH
2	2	6061 AL L-BRACKET, 0.25 IN WIDTH
3	5	20 TOOTH, 2 MM GT2 IDLER PULLEY, 6 MM WIDTH
4	1	20 TOOTH, 2 MM GT2 DRIVING PULLEY, 6 MM WIDTH
5	6	18-8 STAINLESS #10-32 HALF-THREADED SHAFT
6	4	#10-32 NYLOCK
7	4	#10-32 HEX NUT
8	1	PARALLAX FEEDBACK 360 HIGH-SPEED SERVO
9	1	SERVO MOUNT AND BELT TENSIONER
10	1	SHAFT SUPPORT
11	1	18T GEAR
12	1	37T GEAR

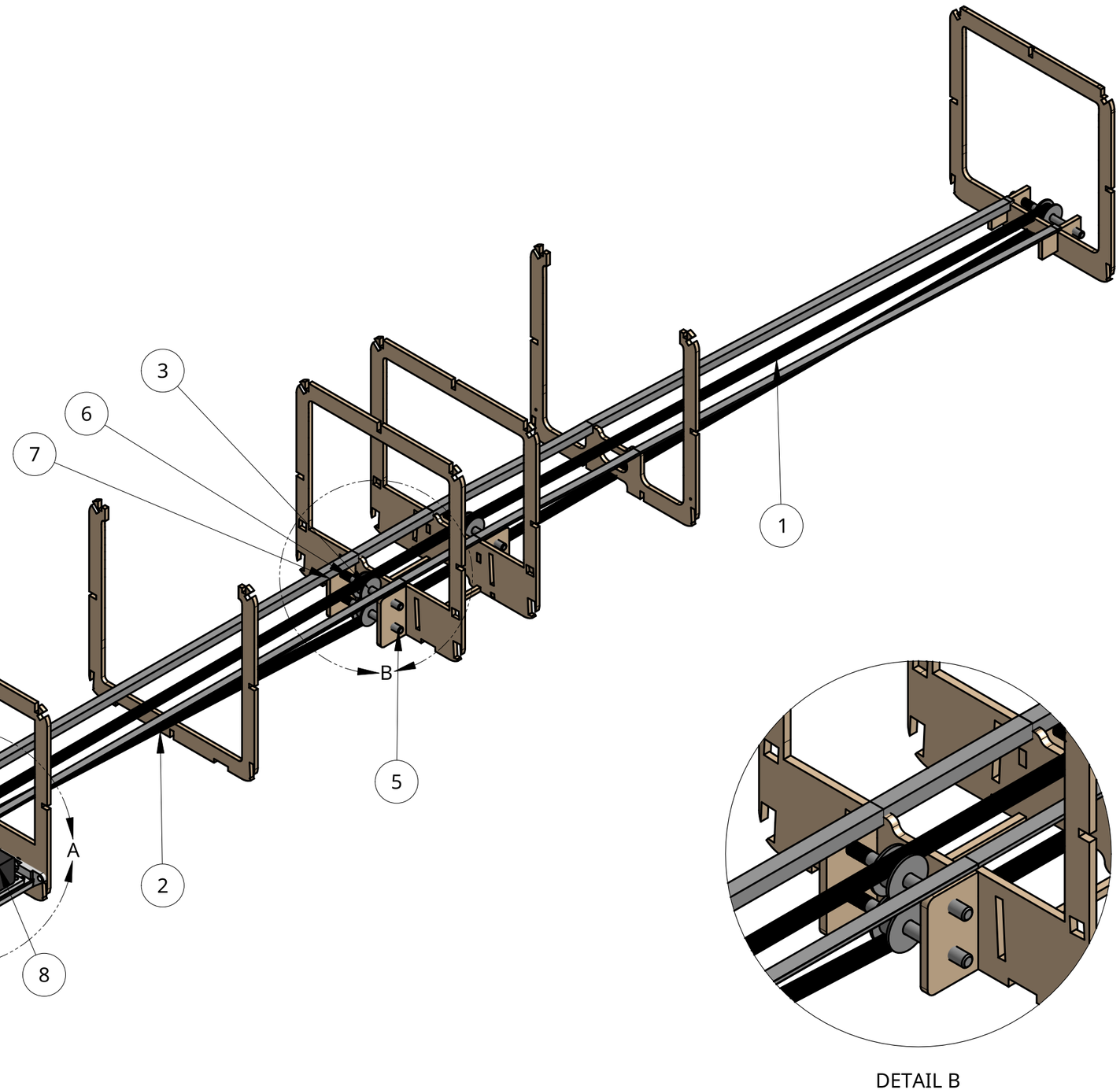

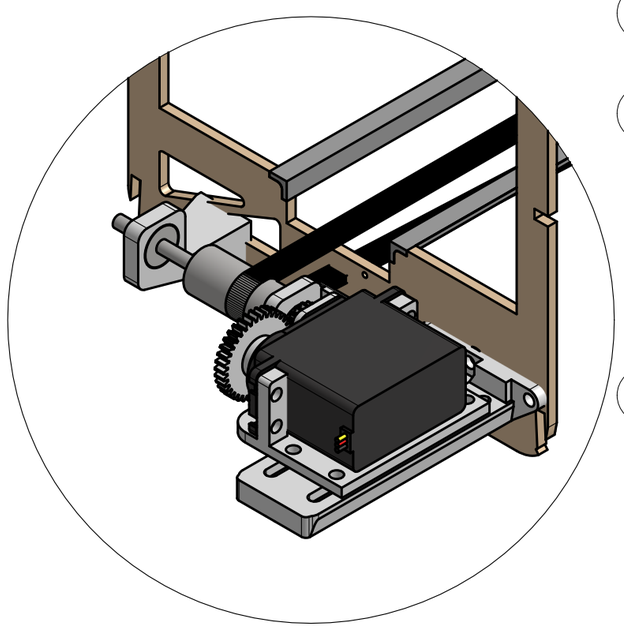

DETAIL A
SCALE 2:3

DETAIL B
SCALE 2:3

DWG NO.	SIZE	SCALE	SHEET	REV.
CONVEYOR SUBSYSTEM	B	1:3	4 of 4	1

6 Manufacturing

Various manufacturing processes were identified and analyzed for the integration of each component and subassembly. The considered and selected manufacturing processes are further discussed in this section.

6.1 Manufacturing Process

6.1.1 Foam Construction

Foam construction of aircraft components allowed for parts with complex geometry to be manufactured quickly and consistently. This method has been utilized in legacy aircraft and is popular for vehicles not subjected to high loading. Foam construction was heavier than some alternatives because large components must be supported by balsa or composite sheeting to maintain structural integrity.

6.1.2 Wood Construction

Wood construction, including balsawood, basswood, and plywood, allowed for the optimization of strength to weight throughout the aircraft structure. Additionally, the use of a high-precision laser cutter allowed parts to be fabricated quickly and accurately to uphold design specifications. Although wood components could have been the most difficult to assemble, proper manufacturing training and techniques mitigated this issue.

6.1.3 Composite Construction

Composite materials were useful when components of a high strength-to-weight ratio were required. With care for proper design and layup, composites could have been implemented strategically to reinforce parts subjected to high loading without significantly increasing the aircraft mass. However, the added cost and complexity inherent to composite manufacturing had to be considered throughout the build process.

6.1.4 3D Printing

While 3D printing was not suitable for a complete aircraft, it allowed for components that were too small or complex for other manufacturing methods to be fabricated. This technique was time intensive and prone to failure but produced precision parts that were unobtainable by other means. 3D printing also provided aerodynamic contours where structural integrity of the component was less of a concern.

6.1.5 Selected Manufacturing Process

A decision matrix, given in Table 6-1, was used to select the best manufacturing process for the primary aircraft structures of the fuselage, wing, and tail. Wood construction was selected to assist in meeting Requirement AC-05 by building the lightest aircraft possible.

Table 6-1: Manufacturing process selection decision matrix

Criteria	Weight		Wood	Foam	Composite
Weight	3	27.3%	5	2	3
Strength	3	27.3%	3	2	5
Product Designability	2	18.2%	3	5	4
Manufacturability	2	18.2%	5	4	3
Cost	1	9.1%	5	4	2
Weighted Total	**11**	**100.0%**	**4.09**	**3.09**	**3.64**

6.2 Manufacturing Milestones

Gantt charts, shown in Figure 6-1, were utilized to plan the manufacturing of each aircraft iteration. The schedule was refined from each iteration to the next by comparing the plan to the actual schedule. Note that the schedules overlap with weekends and school holidays, resulting in some tasks appearing to take longer than the number of days over which the work was actually performed.

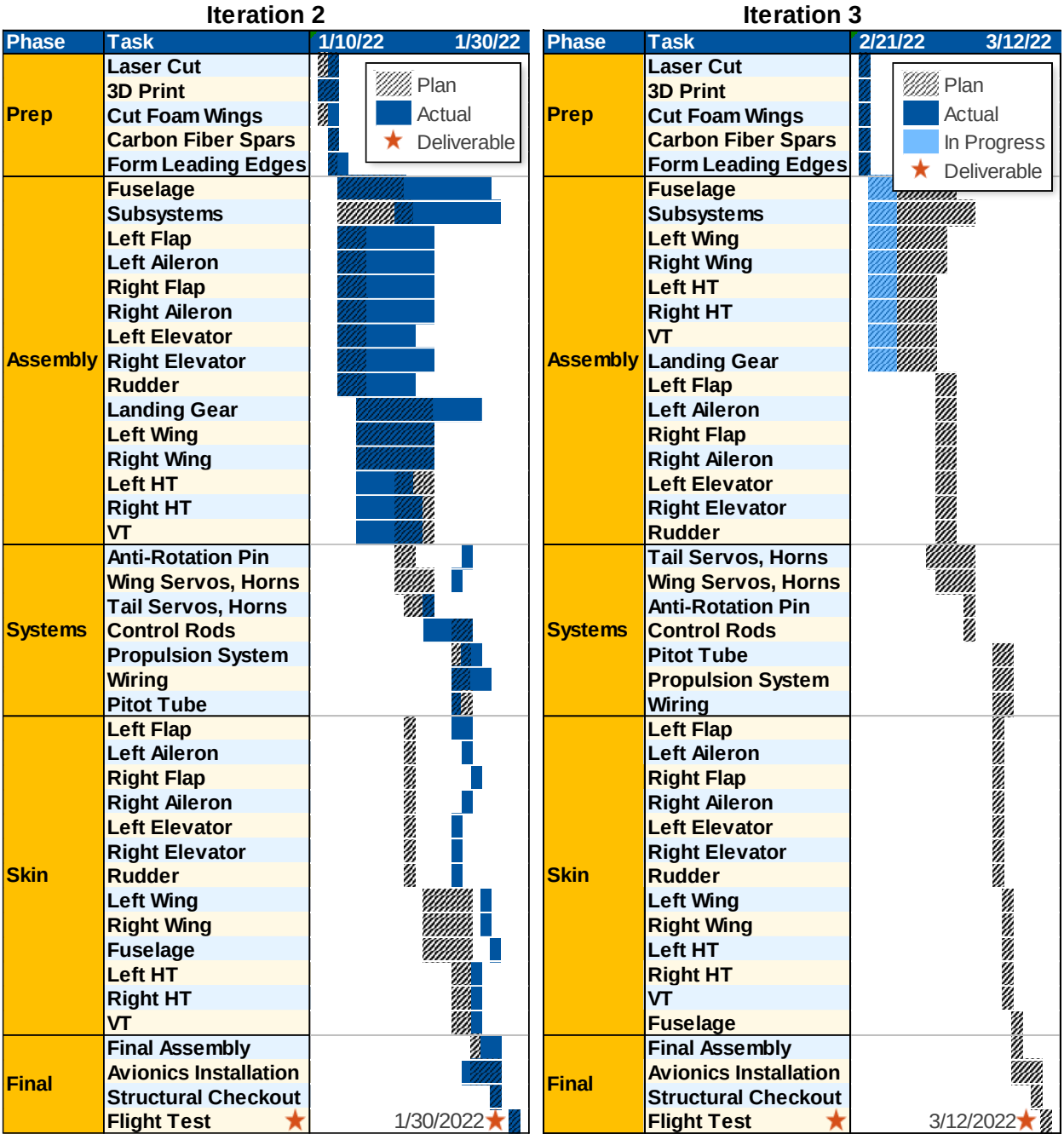

Figure 6-1: Iterations 2 and 3 manufacturing Gantt chart

6.3 Detailed Manufacturing Summary

6.3.1 Wing and Tail Structures

A summary of the selected manufacturing process for each wing and tail component is given in Table 6-2. Epoxy was used to glue all structural components, while cyanoacrylate (CA) glue was used to install the remaining components.

Table 6-2: Wing and tail component manufacturing process summary

Surface	Component	Material	Dimension	Method
HT and VT	Main spar	Carbon fiber	1/4 in by 1/4 in	COTS
Wing	Main spar	Carbon fiber	3/4 in by 3/4 in	COTS
	Aft spar	Basswood	1/8 in thick	Laser-cut
Control Surfaces	Spar	Basswood	1/8 in thick	Laser-cut
Wing, HT, VT, and Control Surfaces	Tip and root ribs	Basswood	1/8 in thick	Laser-cut
	Middle ribs	Balsawood	1/8 in thick	Laser-cut
	Leading edges	Balsawood	1/16 in thick	Laser-cut
	Stringers	Balsawood	1/4 in or 1/8 in thick	Laser-cut
	Skin	MonoKote	N/A	COTS

6.3.2 Fuselage Structure

A summary of the selected manufacturing process for each fuselage component is given in Table 6-3. Again, epoxy was used to glue all structural components, while CA glue was used to install the remaining components.

Table 6-3: Fuselage component manufacturing process summary

Assembly	Component	Material	Dimension	Method
Semi-Monocoque Fuselage	Bulkheads	3-Ply Plywood	1/8 in thick	Laser-cut
	Firewall	5-Ply Plywood	1/4 in thick	Laser-cut
	Longerons	7-Ply Plywood	1/8 in thick	Laser-cut
	Stringers	Balsawood	1/4 in thick	Laser-cut
	Shear Panels	Balsawood	1/16 in thick	Laser-cut
	Skin	MonoKote	N/A	COTS
Wing Box and Tail Box	Wing carry-through interference	Carbon fiber	3/4 in by 3/4 in	COTS
	Remaining components	3-Ply Plywood	1/8 in thick	Laser-cut

6.3.3 Remaining Components

The selected manufacturing processes for the remaining components are explained in Table 6-4.

Table 6-4: Remaining component manufacturing process summary

Assembly	Component	Material	Dimension	Method
Nose Landing Gear	Strut	Steel round stock	3/16 in diameter	COTS, bent in-house
Main Landing Gear	Strut	Carbon fiber	Variable	In-house layup
Wing/Fuselage	Anti-rotation pin	Machine screw and T-nut	10-32 thread	COTS
VT/Tail Box	VT securement to the tail box	Machine screw and T-nut	10-32 thread	COTS

6.3.4 Subsystems

The VSSM and VVPDM were manufactured and integrated with the aircraft using a similar built-up wood method. The hardware for each subsystem, primarily COTS as explained in Section 4.7, was attached to the fuselage using laser-cut basswood, balsawood, and 3D-printed components. The VSSM payload bags were sewn out of a polyester cotton blend fabric and the VVPDM conveyor belt drive servo was secured to the nose landing gear bulkhead with a 3D-printed bracket.

7 Testing Plan

Full aircraft and subsystem testing was performed to validate the design and to improve upon functionality, reliability, and performance. A Pixhawk flight computer was used to record telemetry data including airspeed, groundspeed, altitude, pilot inputs, load factor, power consumption, and more.

7.1 Test Objectives

The test objectives shown in Table 7-1 were established to ensure that all design requirements were met.

Table 7-1: Test Objectives

System	Objectives
Propulsion	Conduct propulsion tests to collect throttle, power consumption, thrust, and airspeed data to validate the designed propulsion performance
	Systematically optimize the battery, motor, and propeller selection to meet Requirements AC-05, AC-12, M2-02, and M3-06
Wing Lift	Conduct wind-tunnel tests on the wing to validate the designed characteristics
	Systematically optimize the wing area to meet Requirement AC-05
Structures	Conduct wingtip loading tests to meet Requirement AC-02, validate the wing spar FEA, and locate potential points of failure in the aircraft structure
	Conduct wing box and wing carry-through destructive tests to validate the FEA
	Conduct fuselage deflection tests to evaluate the improvement from shear paneling
	Conduct landing gear deflection tests and record all landings to validate the FEA
Vaccine Syringe Storage	Systematically optimize the number of syringes able to be stored in the aircraft to maximize the Mission 2 score while balancing the overall aircraft performance
	Conduct ground tests of the syringe loading to improve the Ground Mission score

System	Objectives
Vaccine Vial Package Delivery	Systematically optimize the number of vial packages able to be delivered to maximize the Mission 3 score while balancing the overall aircraft performance
	Conduct tests of the VVPDM to validate its reliability and ensure a proper CG is maintained

7.2 System Testing

7.2.1 Propulsion

To validate and optimize the propulsion system selection, a series of static thrust tests were performed with various combinations of motors, batteries, and propellers using the setup shown in Figure 7-1. Performance parameters were then recorded and compared to the manufacturer's specifications to select a propulsion system combination that provided sufficient static thrust to meet Requirement AC-05. In addition to static thrust tests, dynamic tests were performed by placing the static thrust test stand on the top of a vehicle to optimize the cruise airspeed and endurance for Requirements AC-12, M2-02, and M3-06.

Figure 7-1: Static thrust test setup

Once the static and dynamic propulsion test data was gathered, they were then compared to theoretical propeller thrust values and those collected during test flights. The goal of these comparisons was to determine a throttle percentage that allowed MULLET to fly as fast as possible for the designed 8-minute in-air flight time seen in Mission 3.

7.2.2 Wing Lift

A full-scale, semi-span wing model, shown in Figure 7-2, was tested at takeoff and cruise conditions in the ERAU DB low-speed wind tunnel to analyze the designed aerodynamic characteristics. A splitter plate isolated the wing from the wind tunnel boundary layer. In addition, flight tests were performed to validate that the wing provided the required maximum lift for takeoff.

Figure 7-2: Full-scale wing model in the wind tunnel; SD7062 profile with 7.5-degree flap deflection (top)

7.2.3 Structures

Structural tests were performed on the aircraft to ensure that it could handle all expected loads. Wingtip load tests were first completed to simulate a 2.5 g load factor, as shown in Figure 7-3. The fuselage and landing gear were also tested to validate that they would carry the expected limit loads.

Figure 7-3: Wingtip load test

Next, the wing box and wing carry-through were destructively tested to validate that the structure could handle a 5 g load factor, as shown in Figure 7-4. To simulate the bending moment and shear, the test article was supported on the spars at the spanwise location of the resultant lift force with a downward vertical load placed on the wing box. Two supports constrained either side of the wing box to allow vertical deflection while limiting deflection and twist in any other axis due to unequal loading in the test setup.

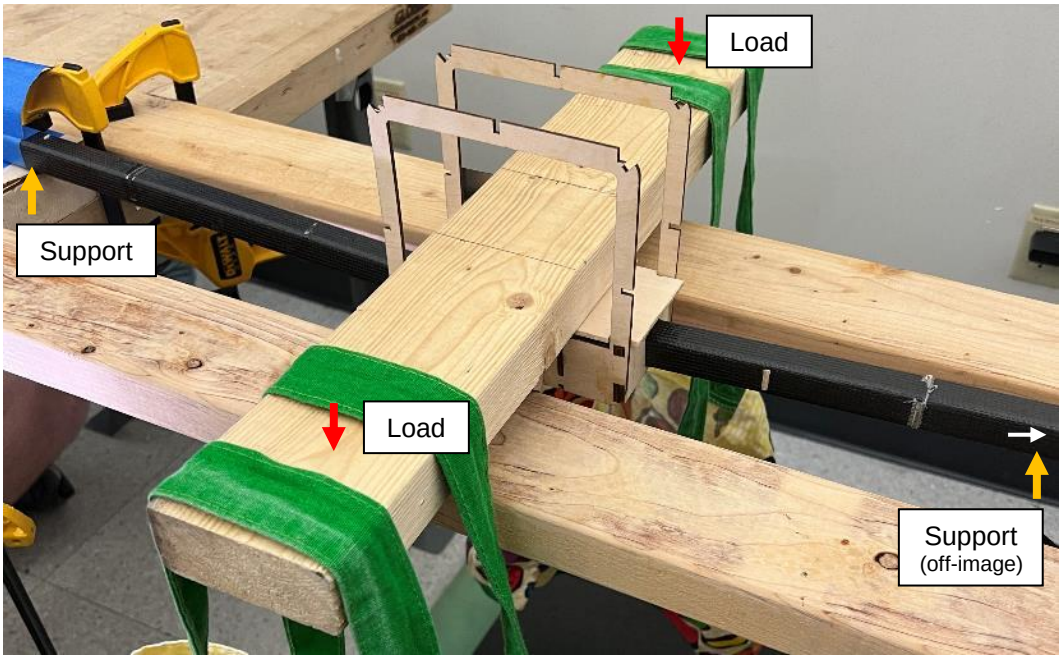

Figure 7-4: Wing box destructive test setup

7.2.4 Vaccine Syringe Storage

Extensive ground tests of the VSSM were conducted in the fuselage payload bay to ensure that the designed payload of 105 syringes could be stored for Mission 2. The loading and unloading times were also tested to minimize the Ground Mission time. Additionally, flight tests were performed to test the aircraft's ability to carry more payload in an effort to maximize the Mission 2 score.

7.2.5 Vaccine Vial Package Delivery

To demonstrate that the VVPDM could carry the desired payload of eight vial packages, thorough ground and flight tests were performed to evaluate the system's reliability, feasibility, and Mission 3 score performance. The prototype fuselage shown previously in Figure 4-8 was used extensively to test the subsystem in various configurations, including ground shake tests and CG checks to ensure in-flight safety. Testing of the VVPDM culminated in an optimization of the number of vial packages to maximize both the Ground Mission and Mission 3 scores.

7.3 Test Checklists

The following checklists in Table 7-2 were implemented and utilized during all applicable ground and flight tests. These checklists ensured safety and redundancy during all tests.

Table 7-2: Test checklists

Ground Inspections	
Fuselage	
Visual inspection	Pass
Aircraft skin tear-free	Check
Servos, linkages, horns	Secure
Wings, ailerons, flaps	Secure
Tail, elevators, rudder	Secure
Landing gear	Secure
Motors	
Motor & firewall	Secure
Propeller damage-free	Check
Prop. nut & direction	Correct
Interior	
Battery voltage	Check
Antennas	Correct
Servo, receiver plugs	Secure
Syringes (if req'd)	
VSSM	Secure
Syringes	Install
Payload not free to move	Check
Vial Packages (if req'd)	
VVPDM	Configured
Door slide	Secure
Vial packages	Install
Payload not free to move	Check

Flight Crew Inspections	
Pre-flight	
Propulsion batteries	Install
Receiver batteries	Install
CG location and weight	Check
Wingtip test	Pass
Receiver switch	On
Control surface directions	Correct
Range check	Pass
Radio failsafe	Correct
Throttle down and safe	Check
Arming plug	Arm
Propulsion run-up	Pass
Arming plug	Disarm
Wind direction & runway	Chosen
Pilot ready to fly?	Go/No-Go
Throttle down and safe	Check
Arming plug	Arm and fly!
Post-flight	
Throttle down and safe	Check
Arming plug	Remove
Propulsion batteries	Unplug
Receiver batteries	Unplug
Walk-around aircraft	Complete
Debrief	Complete

7.4 Test Schedule

Table 7-3 summarizes the completed and planned tests through the competition fly-off in April 2022.

Table 7-3: Completed and planned tests

Date	Type	System	Objectives
10-11-21	Ground	Wing Lift	Full-scale, semi-span wing wind-tunnel test
10-13-21	Ground	Propulsion	Initial thrust tests of battery and motor performance
10-30-21	Flight	All	Iteration 1 maiden, aircraft trim, stability and control
11-02-21	Ground	VVPDM, VSSM	Initial demonstration of subsystem prototypes
11-11-21	Flight	All	Envelope expansion, stall characteristics
11-13-21	Flight	Lift, Propulsion	Takeoff performance, weight envelope expansion
12-08-21	Ground	VVPDM	Full demonstration of conveyor belt and door slide
12-10-21	Ground	Propulsion	Dynamic thrust tests to validate motor and propeller
01-21-22	Ground	Structures	Shear panel and landing gear deflection tests

Date	Type	System	Objectives
01-29-22	Flight	All	Iteration 2 maiden, evaluate takeoff performance
02-04-22	Ground	Propulsion	Static thrust tests to validate motor and propeller
02-12-22	Flight	All	Flight demonstration of Missions 1, 2, and 3
02-16-22	Ground	Structures	Wing box destructive test
02-19-22	Ground	VVPDM	Test safe CG during/after payload deployment
02-26-22	Flight	VVPDM	In-flight demonstration of Mission 3 payload delivery
02-27-22	Ground	Propulsion	Full Mission 3 battery endurance test
03-05-22	Flight	All	Mission performance refinement
03-12-22	Ground	VVPDM, VSSM	Full validation of subsystems
03-26-22	Flight	All	Iteration 3 maiden, test competition readiness
04-02-22	Flight	All	Pilot and ground crew practice, detail modifications
04-09-22	Flight	All	Pilot and ground crew practice, detail modifications
04-16-22	Flight	All	Final aircraft certification for fly-off

8 Performance Results

The previous testing plan was used to obtain data to evaluate the designed performance. The following section describes and discusses the results of all ground and flight tests.

8.1 Systems

8.1.1 Propulsion

Figure 8-1 shows the static thrust results for the M6 Code 12 400Kv motor with an APC 15x10E & APC 16x10E propeller, different voltages for the propulsion system were tested and compared to the APC manufacturer provided static thrust data [22].

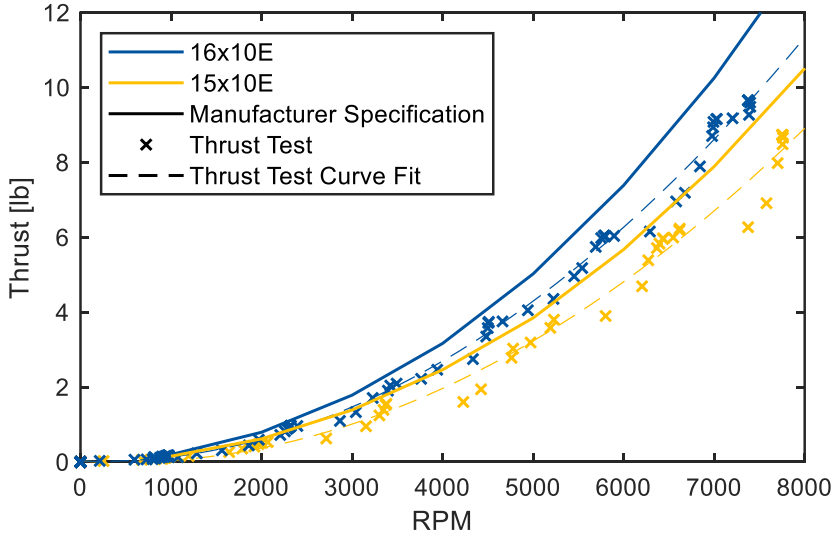

Figure 8-1: Experimental and theoretical static thrust versus RPM for the APC 15x10E propeller [22]

In addition to static thrust tests, dynamic thrust and endurance tests further validated the propulsion system's selection. Flight tests indicated that the actual battery draw was significantly less than that estimated for Mission 3 (67.7 Wh versus 83.0 Wh, respectively). These tests indicated that the optimal throttle input for Mission 3 was 62%. Finally, the propulsion tests allowed for the refinement of the mission propeller selections, shown in Table 8-1. The APC 16x10E performed the best for all missions. However, at the lower gross weight for Mission 1, it was determined through flight that the APC 16x12E provided better flight performance.

Table 8-1: Propeller selections based on propulsion tests

Mission	M1	M2	M3
Propeller	APC 16x12E	APC 16x10E	APC 16x10E

8.1.2 Wing Lift

The lift and moment results from the wind-tunnel experiment are shown in Figure 8-2. Table 8-2 compares the design values to the experimental data gathered from the wind-tunnel test, revealing where further analysis was required. The wind-tunnel experiment was performed at a chord Reynolds number of 200,000, just below that expected for the aircraft during takeoff (250,000). Note that the pitching moment coefficient is reported about the quarter-chord.

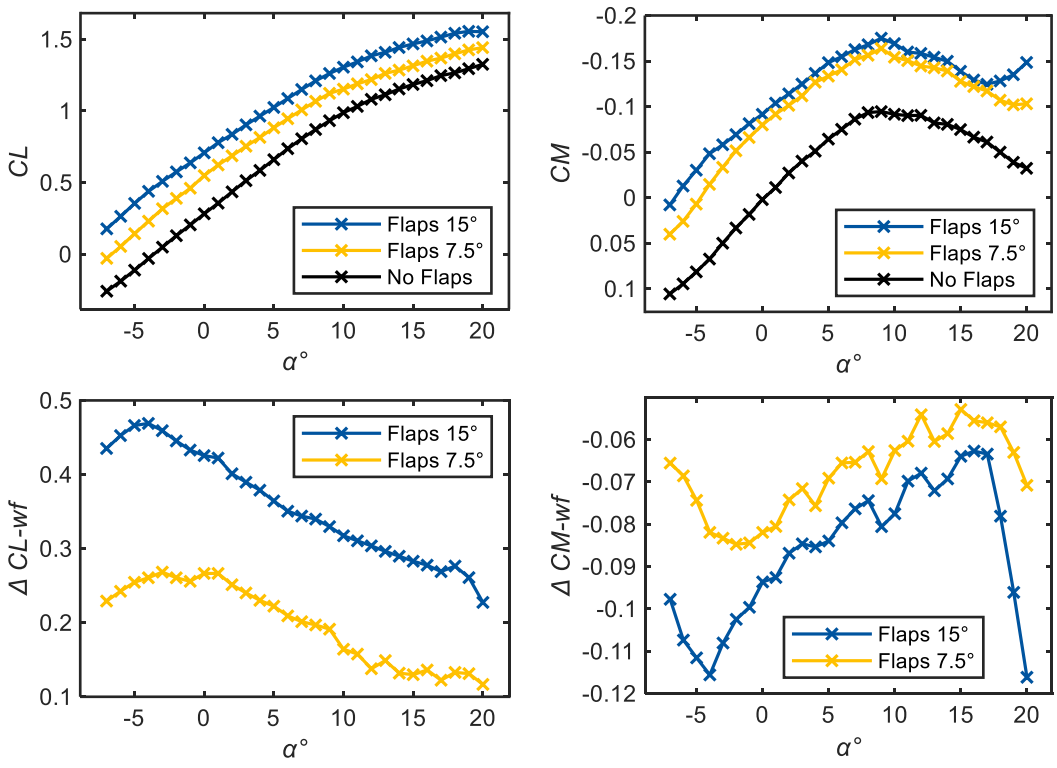

Figure 8-2: Wing wind-tunnel test results

Table 8-2: Wing design parameters compared to wind-tunnel

Parameter	Design	Wind-Tunnel	Difference
$C_{L\text{-}max}$	1.29	1.32	+ 2.33%
$C_{L\text{-}max\text{-}wf}$	1.72	1.56	- 9.30%
α_{0L} [deg]	-3.4	-3.7	+ 8.8%
$\alpha_{0L\text{-}wf}$ [deg]	N/A	< -5	N/A
$C_{L\alpha}$ [/deg]	0.077	0.0748	- 2.9%
$C_{L\alpha\text{-}wf}$ [/deg]	N/A	0.0667	N/A
$\Delta C_{L\text{-}wf}$ (max)	0.433	0.47	+ 8.6%
$\Delta C_{L\text{-}wf}$ (takeoff)	0.433	0.30	- 31%

The wind-tunnel test indicated that the actual lift coefficient with flaps may be lower than that designed. This result prompted further analysis because the wing was sized to takeoff in 25 ft (per Requirement AC-05) based on achievable lift coefficient. However, the propulsion tests previously explained, in addition to further flight tests, revealed that the available static thrust would compensate for any decrease in lift during takeoff. Ultimately, after flight testing, the aircraft repeatedly met the takeoff requirement at all weights.

8.1.3 Structures

During destructive testing, the wing spar failed at 122 lb of lift (a 9.8 g load factor); this failure occurred before the wing box and wing carry-through structure failed. This load amply exceeded the design ultimate load factor of 5 g, validating the FEA results and allowing the continued expansion of the aircraft's weight envelope. Figure 8-3 compares the wing spar deflection during the wing box destructive test to the FEA, and Figure 8-4 shows the outcome of the wing box destructive test.

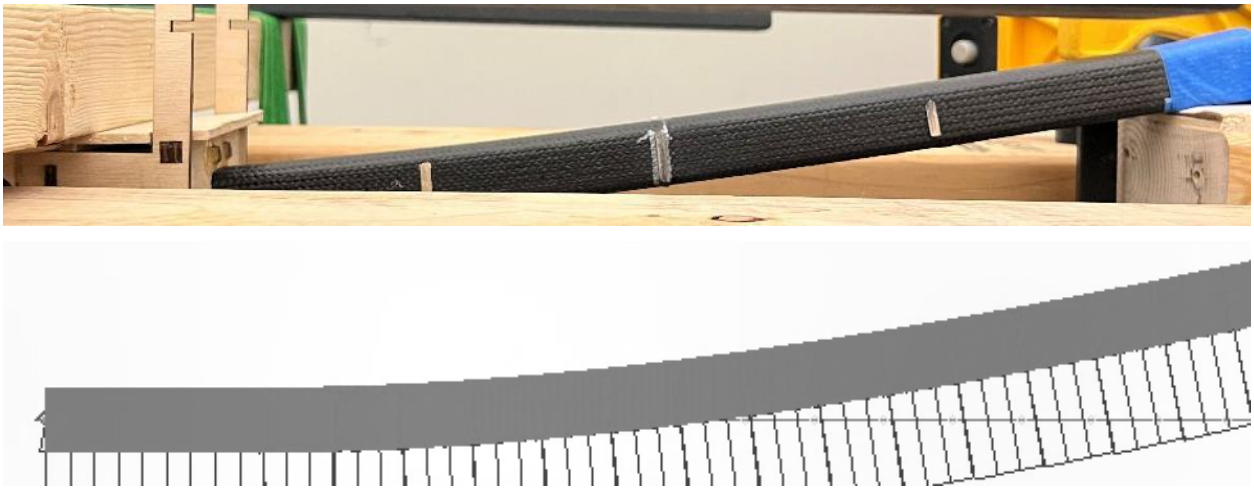

Figure 8-3: Wing spar deflection compared to FEA (FEA deflections not to scale) [17]

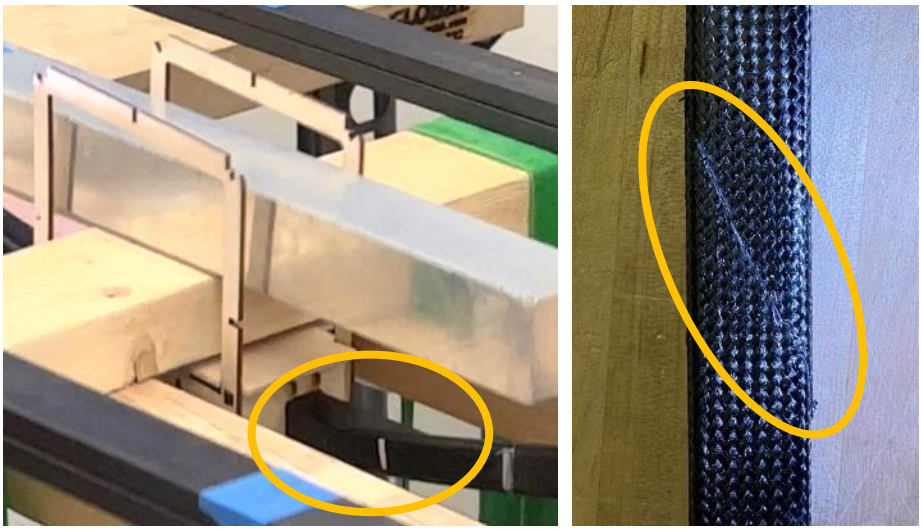

Figure 8-4: Wing box destructive test result (spar failure)

Next, the aircraft passed a wingtip test simulating an approximate 2.5 g load factor, as shown previously in Figure 7-3; this test was repeated successfully before all flight tests. In addition, Figure 8-5 shows the wing deflection in a 60-degree bank at a 2 g load factor. These tests proved that the aircraft could withstand, with significant margins, all the loads expected during high-performance maneuvers in testing and competition flight.

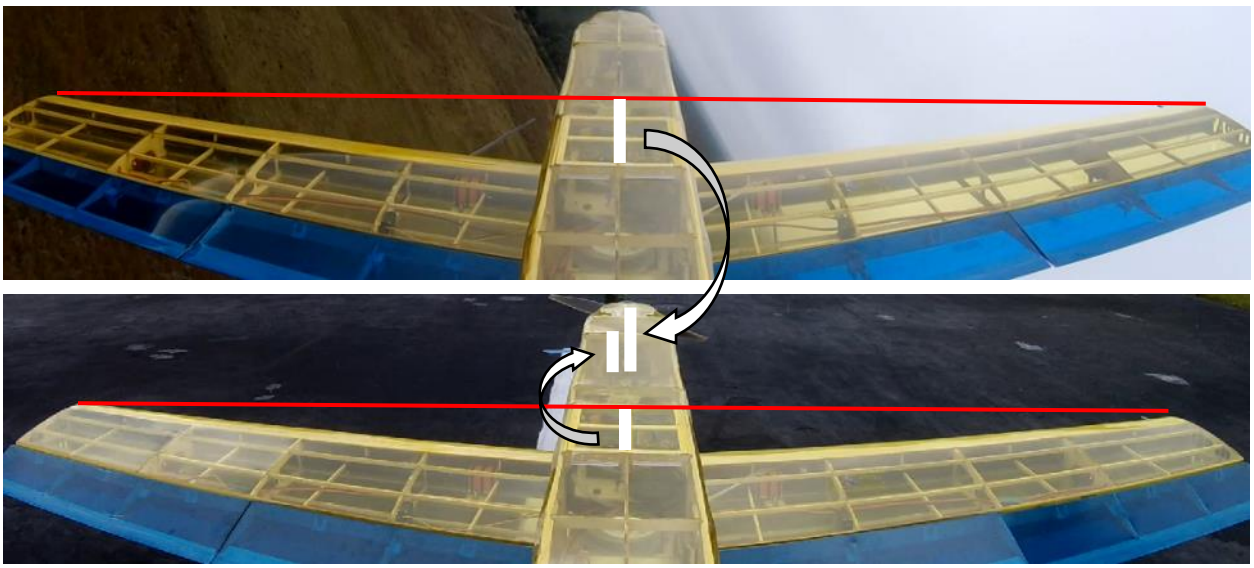

Figure 8-5: Wing deflection in a 60-degree bank (top) compared to on the ground (bottom)

In addition to the extensive wing structure testing, the fuselage shear panels and main landing gear were tested. With a 1-lb load placed on the empennage before and after shear panel installation, the shear panels provided an 83% improvement to the empennage deflection from shear. Then, in the main landing gear deflection test, the gear was measured to have a deflection of 0.26 in (compared to 0.58 in estimated by FEA, Section 5.2.3) when the aircraft was ground-loaded to a 2 g load factor in the heaviest configuration. However, the FEA indicated that the 0.58 in deflection would occur at 5% of the material's ultimate strength.

Therefore, MULLET's fabricated landing gear is likely much stronger than required and could be optimized to further reduce weight.

8.1.4 Vaccine Syringe Storage

It was first validated that the VSSM could fit the designed Mission 2 payload of 105 syringes. Subsequent ground and flight tests further confirmed that the bagging technique was secure and did not shift in-flight. Additional takeoff performance and endurance testing indicated that the airframe may be able to support a greater gross takeoff weight. Combined with the fact that the actual empty weight of MULLET was less than the designed weight, the team estimated that the Mission 2 payload could be increased to 115 syringes to improve the Mission 2 score. To fit this increased number of syringes, the fuselage height of MULLET was increased. The stability and control, drag, weight, and performance characteristics due to this possible change were analyzed with no adverse effects noticed. Further flight testing will help determine the best course of action.

Lastly, multiple ground tests were performed to continuously improve the Ground Mission loading method. The following times were achieved: 22 seconds to load and 8 seconds to unload the syringes.

8.1.5 Vaccine Vial Package Delivery

Utilizing an early fuselage protype, the VVPDM conveyer belt and door slide concept was mechanically tested to confirm the belt and 3M VHB tape's ability to deploy the vial packages. Various ground shake tests showed that the VVPDM could secure the vial packages and maintain a stable CG. In addition, the most extreme vial package placements were tested, verifying MULLET's ability to maintain proper orientation during deployment. Additionally, the VVPDM reliably deploys the vial packages without exceeding the 25 g load factor in any axis per Requirement M3-07.

The vial package loading was practiced to reduce the time to 10 seconds, resulting in a total Ground Mission time of 40 seconds. This time, paired with the increased number of syringes mentioned previously, provides a competitive overall competition score.

8.2 Complete Aircraft Performance

Performance results at the time of writing have been compiled in the following tables. Table 8-3 details specific aircraft performance regarding scoring parameters and competition requirements. Table 8-4 summarizes the team's final scores.

Table 8-3: Complete aircraft design versus actual performance

Mission	Parameter		Design	Actual	Difference
All	Empty Weight [lb]		6.60	5.69	- 13.8%
	Maximum Wing Load Factor [g]		5.0	9.8	+ 96%
	Takeoff Airspeed [ft/s]		33.4	30.4	- 8.9%
	Static Thrust [lb]		10.0	9.8	- 2%
M1	Gross Takeoff Weight [lb]		8.15	7.21	- 11.5%
	Ground Roll [ft]		6.3	8	+ 27%
	Rate of Climb [fpm]		1800	2111	+ 17%
	Cruise Airspeed [ft/s]		110.0	107.4	- 2.4%
	Air Lap Time [s]		30	31	+ 3.3%
	Mission Time [s]		90	94	+ 4.4%
M2	Gross Takeoff Weight [lb]		12.46	11.72	- 5.9%
	Ground Roll [ft]		23.6	18	- 24%
	Cruise Airspeed [ft/s]		110.0	114.6	+ 4.2%
	Air Lap Time [s]		30	28	- 6.7%
	Mission Time [s]		90	91	+ 1.1%
	# of Syringes Carried		105	115	+ 9.5%
M3	Gross Takeoff Weight [lb]		12.20	11.76	- 3.6%
	Ground Roll [ft]		20.7	16	- 23%
	Cruise Airspeed [ft/s]		92.4	94.4	+ 2.1%
	Energy Consumption [Wh]		83.0	67.7	- 18.4%
	Average In-Air Power [W]		637.5	545.5	- 14.4%
	Lap Time [s] (Averaged across all 9 laps)	Total	75	53	- 29%
		Air	60	41	- 32%
		Ground	15	12	- 20%
	# of Vial Packages Delivered		8	9	+ 13%

Table 8-4: Final team scores

Mission	Design	Actual	Difference	Est. Fly-Off Maximum	Final Team Score
M1	Pass	Pass	N/A	N/A	1.00 (Equation 3-1)
M2	70 syringes per minute	76 syringes per minute	+ 8.6%	98 syringes per minute	1.78 (Equation 3-2)
M3	8 successful deployments	9 successful deployments	+ 13%	10 successful deployments	2.90 (Equation 3-3)
GM	30 seconds	40 seconds	+ 33%	15 seconds	0.38 (Equation 3-4)
Total	**N/A**	**N/A**	**N/A**	**N/A**	**6.06**

8.3 Conclusion

This year, the ERAU DB team has consistently improved the rate at which an aircraft can be designed, built, and flown, allowing for rapid iteration of the design to meet the mission requirements. Efficient completion of the conceptual and preliminary design phases in four weeks, followed by the completion of the product design in two weeks, led to a successful wing wind-tunnel test early in the year. The first iteration of MULLET was then manufactured in three weeks, enabling the design's first flight within nine weeks of the requirements being released in September 2021. Two iterations of the aircraft have since been flown on 18 separate flights spanning 1.3 flight hours.

Aside from the full aircraft, concepts of the required subsystems were also demonstrated within the first three months. The vaccine vial package delivery mechanism had successfully deployed vial packages without exceeding a 5 g load factor before the requirement was eased to 25 g in November 2021. In addition, extensive destructive and non-destructive tests of key aircraft structures were performed to validate the FEA from the detail design phase. The successful testing of components and subsystems early in the design process presented the opportunity to continue advancing the performance of the aircraft with the goal of achieving the maximum possible score.

Ultimately, the efforts of the 40-student ERAU DB team culminated in 4,280 manhours dedicated to the design of MULLET, a humanitarian UAV, shown in Figure 8-6. With the actual flight and mission performance meeting or exceeding all designed specifications, including weight, wing lift, static thrust, takeoff distance, cruise airspeed, lap times, payload, and more, the team is confident in their ability to provide a winning performance in the 2021–2022 AIAA DBF competition.

Figure 8-6: MULLET Iteration 2

Bibliography

[1] "2021–22 Design, Build, Fly Rules," *Competition Information*, AIAA, retrieved 24 February 2022. www.aiaa.org/dbf/competition-information/rules-resources

[2] "Airworthiness Standards: Normal, Utility, Acrobatic, and Commuter Category Airplanes," *Code of Federal Regulations*, Federal Aviation Administration, 14 CFR § 23, 2017.

[3] Gudmundsson, S., *General Aviation Aircraft Design, Applied Methods and Procedures*, 1st ed., Butterworth-Heinemann, 2014.

[4] "eCalc," Online Remote-Control Propulsion Sizing Tool, Solution for All Markus Müller, 2021. www.ecalc.ch/motorcalc.php

[5] "AIAA Design Build Fly Competition Summary 2019–20," *Previous Competitions*, AIAA, retrieved 24 February 2022. www.aiaa.org/dbf/previous-competitions

[6] "AIAA Design Build Fly Competition Summary 2020–21," *Previous Competitions*, AIAA, retrieved 24 February 2022. www.aiaa.org/dbf/previous-competitions

[7] Raymer, D. P., *Aircraft Design: A Conceptual Approach*, 6th ed., AIAA, 2018.

[8] "Airfoil Tools," Online Airfoil Database, 2021. www.airfoiltools.com

[9] Ylilammi, N., Gomes Cavalieri, A. V., Soinne, E., "Experimental and Computational Study of Two Flapped Airfoils at Low Reynolds Numbers," Aalto University of Science and Technology, 2010.

[10] Traub, L. W., "Aerodynamic Impact of Aspect Ratio at Low Reynolds Number," *Journal of Aircraft*, Vol. 50, No. 2, 2013, pp. 626-634.

[11] Lyon, C. A, Broeren, A. P., Giguère, P., Gopalarathnam, A., and Selig, M. S., "Summary of Low-Speed Airfoil Data", University of Illinois at Urbana-Champaign, Vol. 3, SoarTech Publications, 1997.

[12] "United States Air Force Stability and Control DATCOM," AFWAL-TR-83-3048, 1978.

[13] Greiner, G., "AE 413 – Aircraft Stability and Control", Embry-Riddle Aeronautical University, 2021.

[14] "XFOIL," Airfoil Analysis Tool, 2021. web.mit.edu/drela/Public/web/xfoil

[15] "United States Air Force Stability and Control Digital DATCOM," AFFDL-TR-79-3032, 1976.

[16] "Surfaces Pro", Vortex Lattice Method Solver, Flight Level Engineering, 2021.

[17] "Finite Element Modeling And Postprocessing," Advanced Simulation Application, Siemens, 2022.

[18] "Design of Wood Aircraft Structures," United States Department of Defense, ANC-18, 1951.

[19] "Tube Fabric Technical Data," Rockwest Composites, 2022. www.rockwestcomposites.com/45355

[20] "12K Carbon Fiber Tow Properties," ACP Composites, 2022. store.acpcomposites.com

[21] Onshape, Computer-Aided Design, Parametric Technology Corporation, 2022. www.onshape.com/en

[22] "Performance Data", Advanced Precision Composites, 2021. www.apcprop.com/technical-information/performance-data